On the relation between solar wind, pseudobreakups and substorms

A. Kullen[1,2]
[2] now at Swedish Institute of Space Physics, Uppsala, Sweden

T. Karlsson[1]
[1]Alfvén Laboratory, Royal Institute of Technology, Stockholm

Short title: PSEUDOBREAKUP AND SUBSTORM STATISTICS

Abstract. A statistical study of pseudobreakups and substorms is performed using Polar UV images from a three-month period in winter 1998-1999. Data from the ACE solar wind monitor are examined in order to determine the influence of solar wind parameters on the occurrence of different substorm and pseudobreakup types.

The results confirm that the IMF clock angle and the amount of solar wind energy flux control the strength of a substorm. The majority of large substorms appear when the IMF is strongly southward and the solar wind energy flux is high. Most small substorms occur during weakly positive or zero IMF B_z and low solar wind energy flux values. Pseudobreakups are associated with even lower energy fluxes than small substorms and appear typically for weakly positive IMF B_z. These results are in agreement with the scenario that pseudobreakups essentially are very weak substorms.

Pseudobreakups appear during quiet times, during the growth phase or the recovery phase of weak or medium strong substorms. Time periods of enhanced geomagnetic activity with recurrent substorms are devoid of pseudobreakups. A detailed analysis of the different pseudobreakup types reveals that quiet time pseudobreakups appear predominantly during northward IMF. At least 20 percent of these appear at the poleward oval boundary. Optically, they do not differ much from very weak substorms. Growth phase pseudobreakups develop typically at the end of a one to two hour long excursion from northward to weakly southward IMF and are followed by quite weak substorms. A large majority of recovery phase pseudobreakups occur at a strongly polewardly displaced oval boundary at the end of a very active recovery phase. A considerable decrease of the polar cap size during the preceding substorm is connected to a northward turning of the IMF.

Introduction

Auroral signatures of substorm activity

The typical phases of an auroral substorm as first described by *Akasofu* [1964] include a local auroral intensification in the nightside oval (onset) followed by an expansion (expansion phase) and a recovery towards the ground state of the auroral oval (recovery). Later, it was discovered that substorm onset is preceded by a 30-60 minutes long growth phase during which the auroral oval expands towards lower latitudes [*McPherron*, 1972]. The onset starts at the equatorward-most discrete auroral arc. The developing auroral surge expands in poleward and westward direction (westward traveling surge). When the intensification region reaches the poleward oval boundary, the boundary may expand as well. Sometimes, multiple substorm expansion onsets can be observed. Many authors claim that the westward traveling surge in fact consists of subsequent onset intensifications that are more and more duskwardly displaced [e.g., *Rostoker et al.*, 1980]. Even during other substorm phases, localized auroral intensifications can be seen. Multiple auroral intensifications at the poleward oval boundary are quite common during substorm expansion and recovery [*Lyons et al.*, 1999]. They often occur repetitively with a time period of 10-15 minutes and many of them involve an equatorward motion and develop north-south aligned structures, also called auroral streamers [*Henderson et al.*, 1998].

The level of auroral activity during a substorm and the size of the auroral expansion can vary considerably. One indicator of the substorm strength is the AE index, measuring the ground magnetic disturbance at 12 stations in the auroral zone. Another indicator of the substorm strength is the size of the auroral oval during substorms. A larger oval size is connected to increasing auroral activity [*Feldstein and Starkov*, 1967], increasing geomagnetic activity [*Hardy et al.*, 1985; 1987] and increasing energy deposit into the magnetosphere [*Fuller-Rowell and Evans*, 1987]. During magnetic storms, the oval is extremely expanded, and long sequences of substorms may occur with peak AE values of 1000 nT or more. During quiet times, the oval is contracted and substorms are commonly rather small (maximum AE about 150-300 nT), although there exist occasionally even stronger substorms during quiet times [e.g., *Henderson et al.*, 1996].

There are substorm-type like auroral activations where the evolution deviates considerably from the three substorm phases. Occasionally, substorms have no clear recovery phase. Instead, a several hours long state of continuously enhanced auroral activity follows the substorm expansion, but with similar auroral signatures as during recovery: auroral intensifications or bulges along the poleward oval boundary, double oval structures and/or auroral streamers. A prolonged recovery that does not return to the ground state is also called steady magnetospheric convection (SMC) event, as it involves a several hours long period of strongly enhanced convection [*Sergeev et al.*, 1996a]. SMC's are a common feature during magnetic storms where extremely strong and turbulent auroral activity continues for up to 1-2 days. Often, classical substorms appear only at the begin and end of a magnetic storm [*Rostoker*, 2002]. During the storm, strong auroral expansions alternate without clear onset and expanding bulge signatures. The recovery of the old expansion region has often not declined yet while a new oval expansion starts [*Pellinen et al.*, 1992].

Not all auroral breakups are followed by a global expansion, but subside soon after the onset. This type of auroral intensification is referred to as a pseudobreakup [*Elvey*, 1957; *Akasofu*, 1964]. Pseudobreakups are short-lived (5-16 min) and can have a longitudinal extension of several hours magnetic local time (MLT)[*Aikio et al.*, 1999]. As most studies focus on pseudobreakups that appear some tens of minutes before substorm onset [*Koskinen et al.*, 1993], they are often discussed as a substorm growth phase phenomenon. However, pseudobreakups occur also during SMC events, substorm recovery [*Sergeev et al.*, 1986; *Aikio et al.*, 1999] and quiet times. *Sergeev et al.* [1986] and *Fillingim et al.* [2000] showed sequences of successive pseudobreakup brightenings during quiet times. The location of a pseudobreakup with respect to substorm onset and oval position can vary. Most growth phase pseudobreakup events have been observed poleward of the following substorm. However, even equatorward [*Nakamura et al.*, 1994] and westward [*Ohtani et al.*, 1993] onset regions have been reported. A poleward motion of 1-2 degrees and the formation of a vortex structure, similar to substorm breakup have been observed for growth phase pseudobreakups [*Voronkov et al.*, 2003]. At least some of the quiet time pseudobreakups studied by *Fillingim et al.* [2000] seem to appear near the poleward oval boundary, although this is hard to tell from Polar UV images, since they have a rather low resolution. The recovery pseudobreakups observed by *Aikio et al.* [1999] appeared on an arc system that moved quickly from more poleward regions towards lower latitudes. As pointed out by *Rostoker* [1998] and *Aikio et al.* [1999] there exists no clear definition of pseudobreakups. Some authors define only those local (non-expanding) breakups as pseudobreakups, that appear during substorm growth phase [*McPherron*, 1991]. Others require an equatorward onset region [*Lyons et al.*, 1999], no considerable poleward motion of the breakup [*Voronkov et al.*, 2003; *Aikio et al.*, 1999] or a short lifetime [*Pulkkinen*, 1996] as additional criterion for a pseudobreakup.

In recent years, several authors have focused on those local auroral activations that appear along the poleward boundary of the nightside oval [e.g., *Lyons et al.*, 1999; *Rostoker*, 2002; and references therein]. According to the definition of poleward boundary intensifications (PBI's), these include multiple brightenings during substorm expansion and recovery phase, auroral streamers, and pseudobreakups that appear near the poleward oval boundary. As could be expected by the inclusion of quiet time and substorm phenomena, PBI's are quite common and appear during all levels of auroral activity [*Lyons et al.*, 1998].

Magnetotail signatures of substorm activity

The auroral signatures of a substorm are accompanied by large-scale changes in the magnetotail topology. Substorm onset is preceded by stretching of the tail (growth phase). The expansion phase is characterized by a thinning of the plasma sheet and magnetic field dipolarization. During recovery the tail returns to its ground state. This cycle is often interpreted as a process of energy loading into the magnetotail via addition of magnetic flux (growth phase) followed by unloading via a substorm [e.g., *Baker et al.*, 1995].

There is no generally accepted model that accounts for all observed features around substorm onset, but it has been agreed on that the initial breakup is connected to a tail current disruption at the inner edge of the plasma sheet at 5-12 R_E from the Earth. The current closes via the westward electrojet through the ionosphere. The formation of a near-Earth neutral line (NENL) is observed further downtail at about 15-25 Re, and is connected to the observed B-field dipolarization and strong earthward plasma flows. According to *Baker et al.* [2002], the current disruption in the inner tail appears as a consequence of the strong earthward plasma flows that brake down in the high-pressure plasma region in the inner tail. Others claim that it is the other way around, a NENL forms as a consequence of rarefaction waves spreading from the current sheet disruption region in tailward direction [*Lui*, 1996].

The plasma flow inside the plasma sheet is not homogeneous. Bursts of local high-speed flows occur in the inner plasma sheet during about $10-15\%$ of the time. Bursty bulk flows (BBF's) last for about 10 minutes and are correlated with local B-field dipolarization and E-field variations. Earthward BBF's are most frequently observed around midnight and earthward of 20 Re. Further downtail, the occurrence rate of tailward BBF's increases, probably due to a NENL location at 15-25 R_E [*Angelopoulos et al.*, 1994]. However, during northward or near zero IMF Bz, earthward BBF's are quite common even in distant tail regions (120-200 Re), indicating a tailward retreat of the reconnection region [*Troshichev et al.*, 1999].

There is a clear correlation between BBF's in the tail and local intensifications in the auroral oval. Several authors showed a connection between BBF's and pseudobreakups [*Berkeley and Kamide*, 1976; *Sergeev et al.*, 1986; *Fillingim et al.*, 2000], auroral streamers [*Henderson et al.*, 1998] and PBI's

[*Lyons et al.*, 1999]. Not all BBF's produce enhanced auroral activity, thus, there is not a one-to-one connection between these [*Fillingim et al.*, 2000]. However, the plasma sheet is more stable and contains fewer and weaker BBF's when PBI's are absent [*Lyons et al.*, 1999].

It is not completely clear to what regions in the tail the different local auroral intensifications map. The source region of substorm onset is found near the inner plasma sheet boundary. Growth phase pseudobreakups are connected to regions further downtail than substorm onset [*Nakamura et al.*, 1994; *Ohtani et al.*, 1993; *Koskinen et al.*, 1993]. The source region of quiet time and recovery pseudobreakups are connected to BBF's in the mid-tail at around 20-40 R_E [*Sergeev et al.*, 1986]. *Rostoker* [1998] pointed out that PBI's must have their source region in the distant tail, as they map to the boundary between open and closed field lines. This is confirmed by *Nakamura et al.* [2001], who showed that BBF's connected to non-poleward pseudobreakups and that small poleward substorm expansions are observed further earthward ($x < 15Re$) than BBF's connected to PBI's and auroral streamers. *Lyons et al.* [1999] reported that PBI's occurring during substorm expansion or recovery are associated with tail dynamics that extends throughout the entire radial extent of the plasma sheet, which could explain their equatorward motion which is often observed.

The influence of solar wind parameters on substorms

There have been numerous empirical studies showing that the occurrence frequency and the strength of substorms are controlled by solar wind parameters. Although there exist substorms that occur during northward IMF conditions, the majority of events appears after a prolonged time of southward IMF [*Kamide et al.*, 1977; *Hsu and McPherron*, 2003]. Looking at long-time averages of the geomagnetic activity, a correlation with the solar wind velocity is found [*Snyder et al.*, 1963]. Southward IMF and a high magnetic energy flux are favorable conditions for large substorms to appear. One of the most commonly used empiric parameters that describe this correlation is the Akasofu-Perreault epsilon parameter $\epsilon = vB^2 sin^4(\theta/2) l_0^2 4\pi/\mu_0$ with v,B and θ denoting the solar wind speed, IMF magnitude and IMF clock angle (θ is defined as the angle between the IMF vector in the yz-plane and the positive z-axis ranging from 0° for pure northward to 180° for pure southward IMF). The constant $l_0 = 7R_E$ gives the linear dimension of the cross section of the solar wind-magnetosphere coupling region. It has been shown in many studies that the epsilon parameter correlates fairly well with the AE index [e.g., *Akasofu*, 1980].

The location of substorm onset is dependent on the IMF. The latitudinal onset position is IMF magnitude and B_z dependent, the MLT position is IMF B_y dependent [*Liou et al.*, 2001; *Gerard et al.*, 2004].

Since a long time there is a debate about whether substorms are a result of an internal instability in the magnetotail or whether they are externally driven by the solar wind. A recent, detailed statistical study by *Hsu and McPherron* [2003] shows convincingly that 60 percent of all substorms are triggered. Around 40 percent of the triggered substorms can be correlated with a northward turning of the IMF (hereafter referred to as IMF norththurn), the others can be associated with an IMF B_y change to zero or a pressure pulse. About 90 percent of the non-triggered substorms occur while the IMF is southward.

Little has been done to examine solar wind conditions during which pseudobreakups appear, at least on a statistical basis. Small-scale auroral intensifications are usually excluded from statistical substorm studies, as the localized signatures do not show up in global parameters such as the AE index or are easily missed in single satellite passes. However, there exists an interesting statistical study by *Zhou and Tsurutani* [2001] which compares solar wind conditions with the nightside auroral activity after a solar wind shock has passed. They found that substorms, pseudobreakups and quiescent (no substorm-activity) events appearing after interplanetary shocks are connected to strongly southward, near zero and strongly northward IMF Bz, respectively.

Models

Pseudobreakups have been found to be associated with the same ionospheric and magnetotail signatures as substorm breakups, the only difference being the global consequence. Magnetic field line dipolarization, energetic particle injections and fast ion flows in the tail can often be as intense as those of substorm onsets, but are short-lived and appear only locally [*Koskinen et al.*, 1993; *Ohtani et al.*, 1993]. For some events, even a local plasmoid formation has been observed [*Aikio et al.*, 1999]. The similarity between pseudobreakup and substorm onset signatures suggests the same physical mechanism behind both phenomena. Many authors claim that there is a continuum of states between pseudobreakups as smallest possible type of substorm and large substorms [e.g., *Aikio et al.*, 1999; *Nakamura et al.*, 1994].

As *Rostoker* [1998] pointed out, it is difficult to distinguish between PBI's, non-poleward pseudobreakups and substorm onset intensifications, as they contain nearly identical auroral and ground magnetic signatures. Even PBI's are associated with magnetic perturbations at geosynchronous orbits and fast flows in the plasma sheet [*Lyons et al.*, 1999]. The high similarity between the different short-term auroral activations has led to the coupled-mode model. *Sergeev et al.* [1996b] and *Rostoker* [1998] both suggested that minor auroral activations represent the basic type of energy dissipation into the ionosphere. This type of substorm activity includes pseudobreakups, substorm onset intensifications, and multiple PBI's during expansion and recovery. The short-term auroral activations occur during all levels of auroral activity and are overlaid on the global, slow-mode substorm activity, that involves global magnetospheric changes and affects the entire auroral oval.

The question remains, why some auroral breakups lead to a global auroral expansion and reconfiguration of the tail, and others not. It has been suggested that auroral enhancements originating in the far tail (PBI's) may involve a different formation mechanism than those occurring near the equatorward oval boundary, like substorm onset intensifications and possibly growth phase pseudobreakups *Rostoker* [2002]. As most growth phase pseudobreakups seem to have a more tailward source region than substorm onset, *Sergeev et al.* [1996b] proposed that impulsive dissipation events have global consequences only when they appear very close to the Earth (the intensity of the dissipation process is largest in the near-Earth tail). Such a scenario does, however, not explain the more tailward source region of substorms occurring on a contracted oval during quiet times [*Lui et al.*, 1976]. *Kan et al.* [1988] and *Lui* [1991] suggested a different scenario: a too low ionospheric conductivity during a pseudobreakup event may prevent a global expansion. However, in several independent studies no difference in the ionospheric conductivity between pseudobreakup and substorm breakup was found [e.g., *Amm et al.*, 2001]. Most authors assume that the rate of the solar wind-energy transfer into the magnetosphere is ultimately responsible for which type of substorm activity occurs. Several authors proposed that growth phase pseudobreakups occur before enough energy is stored in the tail [*Koskinen et al.*, 1993; *Nakamura et al.*, 1994], others speculated that an increasing energy input from the solar wind may prevent a global expansion [*Pulkkinen et al.* 1998; *Rostoker* 1998]. *Partamies et al.* [2003] suggested that a sudden energy decrease may prevent a global expansion during a growth phase pseudobreakup.

Scope of the work

In this work, a statistical substorm study is performed, that is based on Polar UV images and ACE solar wind data. The same data set and method are used as in the statistical study of polar auroral arcs by *Kullen et al.* [2002]. All substorm-like activities that appear during three winter months on the images are selected and compared with solar wind parameters. The main task of this study is to examine solar wind conditions during which local auroral intensifications (outside auroral substorms) appear, and compare them with solar wind conditions during substorms. Knowing the characteristic solar wind conditions for local auroral enhancements will allow to evaluate theories that emphasize the role of the solar wind-magnetosphere energy coupling. For a more detailed examination of local auroral intensifications outside substorm expansion and recovery (here referred to as pseudobreakups), they are sorted into different subgroups depending on their relation to the nearest substorm. In a second categorization, they are classified according to their location within the auroral oval.

Instrumentation

Polar UV images

Polar UV images from a three-month period in winter 1998/1999 (1 December - 28 February) are used for a statistical study of pseudobreakups and substorms. The UV instrument on board the Polar spacecraft produces global images of the auroral regions in the far ultraviolet wavelength range [*Torr et al.*, 1995]. An image is taken every 37 seconds with an integration time of alternately 18 sec or 36 sec. The resolution is about 0.5 degrees, which corresponds to 50x50 km per pixel, and the overall sensitivity is about 10 Rayleigh. The camera is mounted on a pointable despin platform. Thus, in spite of the spacecraft rotation, a constant imaging of the auroral zone is possible for a significant fraction of Polar‘s orbit. During the three months analyzed in this statistics, the UV experiment on Polar provides a global view of the northern auroral oval for approximately 10 hours during each 18-hour orbit time. For another 4 hours, parts of the nightside oval are still visible. This allows a coverage of the auroral activity during about 75 percent of the time. Sheets of 5x6 images have been produced with a time interval between each image of 4 to 6 minutes (an exact determination of the onset time from UV images is difficult due to a low pixel resolution [*Voronkov et al.*, 2003], i.e., smaller time intervals between the images would not improve the accuracy of this study). For a non-biased comparison, all images are done with the same settings: the LBHL long filter is chosen, where wavelengths between 160 and 180 nm are passed. The LBH emissions are the result of excitation of N_2 by electron impact, which are most common at lower layers of the ionosphere at about 120 km altitude. Since the emissions in the wavelengths passed by the filter are not significantly absorbed by the atmosphere, the intensity of the emissions is nearly directly proportional to the electron energy flux into the ionosphere. The integration time is 36 seconds and the color scale reaches from 2 to 20 photons/cm^{2}s such that even weak emissions near the instrument threshold become visible. Two instrument malfunctions slightly reduce the quality of the images. The sharpness of the images is reduced by a periodic wobble of the spacecraft. Perpendicular to the wobble the image resolution is unaffected. In the wobble direction, the images are smeared by a maximum of 10 pixels. Due to a malfunction an aperture door is closed over the lens during 15 percent of the statistical time period. As the door is a transparent MgF window, measurements can still be made when it is closed but the image sensitivity is reduced by about 50 percent. The bad image quality during parts of the time does not affect the results of this study much. The spacecraft wobble prohibits an exact determination of the onset location. On images with reduced sensitivity, extremely weak auroral intensifications may be missed.

ACE Solar wind data

To study the influence of solar wind parameters on the occurrence of the different substorm types, we consider IMF, solar wind speed, and ion density. 5-min averaged data from the ACE solar wind monitor are transformed into GSM coordinates. ACE is located about 220 R_E sunward from the Earth, thus, the solar wind conditions may have changed slightly when reaching the magnetopause. But since ACE has a nearly continuous coverage of the solar wind it is the most suitable satellite to use for this study. The solar wind data are shifted in time to take into account the propagation time of the solar wind to reach the dayside magnetopause (assumed to be located 10 R_E sunward of the Earth). The time delay is calculated for each day using 24-hour averaged solar wind speed and ACE to Earth-magnetopause distance.

AE index

For an estimation of the strength of substorms and pseudobreakups, AE index values are examined. As the final AE index values are not yet available, preliminary data from AE quicklook plots (http://swdcdb.kugi.kyoto-u.ac.jp/aedir/ae1/quick.html) are used and averaged over 5-minute periods. The quicklook plots are derived from only 8 out of the 12 standard AE stations, using unchecked data. In this study, the statistical distribution of AE values, that are averaged of an entire substorm lifetime, is analyzed. Hence, small or short-time deviations from the real AE value do not affect the results. The AE data used in this study contains fairly realistic values for the entire statistical period except for about 30 data points where the values are obviously wrong. These have been excluded from the statistical analysis. The limitation of the AE index as a measure of substorm strength lies in the fixed position of the ground stations. For substorms appearing on a much contracted oval (poleward of the stations), the AE index underestimates the the magnetic disturbances that are correlated with the substorm event.

Method

Classification of events

Every substorm-like activity that appears on the UVI images is selected, even those with onsets much dawn- or duskward of the usual onset region. Excluded from the analysis is the dayside part of the oval between 10 and 14 MLT. For each event, start and end time, the size of the oval and the MLT onset location are marked. These parameters are determined exclusively from visual inspection of the UV images.

As it is not possible to determine the start of the growth phase from Polar UVI images (the equatorward motion of the most equatorward arc is often not seen on the images), auroral substorms are defined here as described in *Akasofu* [1968] and include only expansion and recovery phase. The start of a substorm is defined as the time where the onset is for the first time clearly visible on an UV image. The development between a first, often extremely weak brightening, and a clearly identified onset is in most cases fluctuating and takes several minutes. As *Voronkov et al.* [2003] pointed out, the onset determination from visual inspection of Polar UV images is accurate to within about 5 minutes only. Hence, an inspection of all images would have given an only marginally better result than looking at images with a time span of several minutes between them, as done here.

To define the end of a substorm is difficult, as the auroral signatures of the recovery phases vary enormously between different substorms. The return to the ground state extends from over tens of minutes up to several hours. Here, the last image that shows typical recovery phase signatures before the auroral oval has returned to its non-disturbed ground state, is chosen as the end time. Typical recovery phase activities include double-oval structures, multiple PBI's, auroral streamers, or oval-aligned arcs/filamentary structures at the dusk or dawn oval side that are not yet connected with the equatorward boundary of the nightside oval. Such a definition of the substorm end includes SMC events as part of the preceding substorm. As there is often a gradual transition towards the ground state, the determination the a substorm end can be arbitrary up to tens of minutes. In case several substorm expansions occur after each other without returning to the ground state in between, the end-time of the previous substorm is defined as the onset time of the next substorm. In case the oval is outside the field of view at substorm onset, the first image on which the substorm is seen is taken as the start time of the event. Accordingly the last available image is taken as the end of the substorm.

For a correct calculation of the oval size, the location of the entire poleward and equatorward oval boundaries should be known. As this is not the case, the boundary position at 0 MLT is taken (which is part of the oval region with the longest image coverage per orbit). Being interested in the relative oval size, averaged over one substorm, we simplify the oval size determination by considering only the equatorward oval boundary. It changes much less during a substorm than the poleward boundary. The oval size is defined as small, medium and large in case the position of the equatorward oval boundary is at midnight equatorward of 60 Cglat (corrected geomagnetic latitude), between 60 and 63 Cglat or poleward of 63 Cglat, respectively. In cases where the equatorward oval position increases (decreases) considerably during the course of the substorm (1° Cglat or more), the oval size is defined as expanding (shrinking). The chosen latitudinal ranges for small, medium and large ovals are the best guess from visual inspection. Other latitude intervals could have been taken instead. Tests with different latitude intervals revealed that the qualitative results are not affected by the choice of the intervals.

All substorm-like events identified on the Polar UV images are classified as either pseudobreakups or substorms. Excluded from the statistical analysis are unclear cases such as extremely weak, pseudobreakup-like brightenings (67 cases) and events where no categorization was possible due to an insufficient field-of-view by the imager (68 cases). The term substorm is used here in a wide sense covering all auroral activations that lead to an auroral expansion and recovery, independent of the scale size of the expansion and includes even very small substorms, SMC events and stormtime expansions that show no clear onset signatures. All identified substorms are subdivided into small-oval, medium-oval, large-oval, expanding-oval or shrinking-oval substorms according to the average oval size during the event. Like in the original definition used by *Akasofu* [1964] we identify events as pseudobreakups when a local auroral intensification does not lead to a global expansion. Pseudobreakups include all local auroral activations that are visible in at least one image and appear outside substorm expansion or recovery, independent of their position within the nightside auroral oval. Even quiet time PBI's, auroral intensifications at the nightside connection point of polar arcs, and auroral enhancements appearing directly after a substorm recovery are counted here as pseudobreakups (due to the unclear definition of the substorm end, some of the recovery pseudobreakups could also be defined as still being part of the late recovery phase).

For a more detailed examination of pseudobreakups, they are split into different subgroups depending on their relation to the nearest substorm. Single and growth phase pseudobreakups are differentiated strictly by the time span between pseudobreakup onset and substorm onset. As the growth phase of a substorm typically lasts for several tens of minutes, we define those pseudobreakups as growth phase pseudobreakups that appear within 30 minutes before the next substorm onset becomes visible. A recovery phase pseudobreakup is defined as a single, localized brightening occurring at the very end/directly after a substorm recovery. In cases where substorm recovery decays extremely smoothly such that no clear end time can be defined, the start time of the first appearing pseudobreakup defines the substorm end time.

In a second categorization pseudobreakups are classified according to their location inside the auroral oval as poleward or middle events. Unfortunately, it is not possible to detect equatorward pseudobreakups in Polar UV images. Hardly any of these occur when the oval is thick and on a thin oval, the pseudobreakup location cannot be determined from Polar UVI. Due to the limited resolution in the UV images (aggravated by the spacecraft wobble) pseudobreakups appear to have an extension of several degrees. In case the oval is thin, a pseudobreakup appears to be as wide as the oval itself (see Figure 1a in [*Fillingim et al.*, 2000]. Only those events can be identified as poleward pseudobreakups where the oval is thick, the brightening extends as a small bulge into the polar cap, or it appears on the poleward part of a double-oval structure. This means, the group of poleward pseudobreakups consists exclusively of poleward events, while the group of middle pseudobreakups includes all events that appear on a thin oval and may contain equatorward as well as poleward cases.

Statistical analysis

The distribution of different solar wind parameters and the AE index are examined for each substorm and pseudobreakup type. The statistical results are presented as bar plots that are all done in a similar way. The solar wind parameter values are split into several interval ranges. For each substorm and pseudobreakup, the average solar wind parameter value during the entire lifetime of the event is calculated. The bars in the plot mark for each solar wind parameter interval, the number of events (given in percentages) that have an average value within that interval.

To be able to compare the solar wind parameter distribution of substorms and pseudobreakups with the average solar wind distribution that prevails during the three months examined in this study, dotted lines mark the solar wind distribution typical for the time period studied. For a calculation of the average solar wind conditions during the statistical time period, all 5-min averaged data points of the 3-month period are used, except for the time intervals during which the UV imager did not point toward the auroral oval. For each interval range in the bar plots the number of data points is calculated (in percentages) that have values within that interval.

In Figures 1,8 and 10 the history of the solar wind distribution is shown as well. In these plots, the hourly averaged solar wind parameter values are shown up to 5 hours before and after the events. In Figures 4-6 and 10, the parameter values are divided into four intervals which are chosen so that the solar wind parameter has values within each interval during 25 percent of the statistical time period.

An entirely average distribution of substorms would correspond to four equally long bars that reach the 25%-mark. Binning the solar wind data in this way makes it easy to detect any deviation from the average solar wind distribution during the statistical time period.

With this method the characteristic solar wind conditions of different auroral phenomenon are easily found. The effect of large-scale changes (hours) in the solar wind parameters on the occurrence frequency of the different phenomenon is revealed as well. The examination of possible solar wind triggers for different substorm and pseudobreakup types is not part of this study. The absence of a satellite providing continuously solar wind data near the dayside magnetopause and an only approximate determination of the onset times does not allow such an examination.

Results

Occurrence frequency and lifetime

From the UVI database, 330 pseudobreakups and 419 substorms have been identified and sorted into different subgroups. The substorms consist of 77 small-oval, 149 medium-oval, 38 large-oval, 37 expanding-oval and 118 shrinking-oval substorms. The pseudobreakups are divided into 192 single, 57 growth phase and 81 recovery phase pseudobreakups. Sorting all pseudobreakups after their position inside the auroral oval results in 122 poleward, and 208 middle pseudobreakups.

In about 15 percent of all classified events, the differentiation between substorm and pseudobreakup is ambiguous. Most of these are hybrids between single pseudobreakups and weak substorms. Intense pseudobreakups that have a broad longitudinal extension are hard to distinguish from extremely weak substorms with a short lifetime and small substorm expansion. 29 of the single pseudobreakups and 35 substorms are such hybrid cases. Growth phase and recovery pseudobreakups are not always clearly separated from substorm onset and recovery, respectively. Nine of the growth phase pseudobreakups may in fact be part of multiple substorm expansion onsets, sometimes observed. There are 28 substorms with extremely active recovery phases where it is difficult to decide whether strong poleward boundary intensifications during recovery are seen (9 cases) or a pseudobreakup event takes place after the recovery (19 cases). Many pseudobreakup events that last longer than ten minutes may change their location slightly, have a variable dawn-duskward length and/or fluctuate. When the fluctuation becomes extreme, such that the luminous spot disappears completely for some minutes, the re-brightening is counted as a new event. Such pseudobreakup sequences may in fact each be one long-lived, fluctuating pseudobreakup. For example, there are about 14 sequences of 5 or more pseudobreakups after each other.

Substorms and pseudobreakups have different characteristic lifetimes. A large majority of pseudobreakups appear for less than 15 minutes, one quarter are visible between 30 and 60 minutes and only a few pseudobreakups last for 2-3 hours. The different substorm types occur for a broad range of lifetimes. The average lifetime of small-oval and medium-oval substorms is about 1.3 hours. Large-oval substorms last for about 2.3 hours. Nearly all large-oval substorms have a lifetime of 1.5 hours or more, some last up to 4-5 hours. Shrinking and expanding-oval substorms have a lifetime distributions similar to large-oval substorms. The values given here are only lower limits of the real lifetimes, since in 14 % of the cases the UV images do not cover the entire evolution of the event.

The occurrence frequency of substorms is high. They are present during 50 % of the statistical time period (for the calculation of the occurrence frequency, even unclear events are included). Pseudobreakups appear during at least 9 % of the time (pseudobreakups appearing on one UVI image only, are assumed to have a lifetime of 2.5 minutes). The occurrence rate of pseudobreakups represents a lower limit, as short-term events may have been missed due to the 4-6 minutes interval between each examined image. From *Kullen et al.* [2002], the occurrence frequency of polar auroral arcs is known. Polar arcs (clear polar arcs and small splits) are visible during at least 16 % of the statistical time period. Nearly half of the polar arc events are overlapping in time with substorms or pseudobreakup events. The time during which the auroral oval remains in the ground state where neither substorms nor polar arcs are seen, does not exceed 33 % of the time. This is an upper limit, mainly, because long-lived polar arcs often exist longer than calculated in the statistics (they disappear from the field-of view even when other parts of the oval are still visible and the arc probably still exists).

The dependence of substorms and pseudobreakups on IMF components

In Figure 1 the distribution of positive and negative signs of each IMF component are shown for different substorm groups: static substorms (including all small-oval, medium-oval and large-oval substorms), expanding-oval substorms and shrinking-oval substorms. The left (right) bars give the number of events (in percentages) having a positive (negative) IMF sign. The top black bar shows the IMF sign distributions at the event start, the bottom black bar shows the number of events for which during the lifetime of the event the IMF component has more often a negative or a positive sign. To get information about the typical IMF distribution before and after the events, the hourly averaged distributions up to five hours before and after the events (gray bars on top and on the bottom of the black bars) are shown as well. The left and right dotted lines in each panel show, how many percent of the statistical time period the IMF components have positive and negative values, respectively.

The dotted lines show that IMF B_z is nearly equally distributed between positive and negative signs during the statistical time period. IMF B_x and B_y are most of the time negative and positive, respectively. No correlation between the IMF B_x and B_y component and the three substorm groups is found. All groups have an approximately average IMF B_x and IMF B_y sign distribution, even in the hours before and after the events. However, the IMF B_z distribution deviates clearly from the average distribution. As could be expected, most substorms occur during southward IMF. While static-oval substorms have nearly the same IMF B_z sign distribution for the hours before and after the events, the IMF B_z distribution changes strongly before and after substorms where the oval size changes considerably during the event. Expanding-oval substorms appear some hours after an IMF B_z sign distribution with equally many positive and negative cases, has changed to a majority of southward IMF cases. For shrinking-oval substorms, the opposite change in the IMF B_z sign distribution is seen. For most shrinking-oval substorms, the IMF is southward the hour before the event. The distribution changes at substorm onset towards an increasing number of northward IMF cases until an equal IMF B_z sign distribution is reached. The IMF B_z distribution shift in time can be explained by the oval size dependence on the IMF B_z component. A southturn or increasingly southward IMF is expected lead to an expansion of the oval, a northturn or decreasingly southward IMF will cause an oval contraction.

Figure 2 shows the IMF sign distribution for the original substorm types. The plots show the distribution of the average IMF values during each event for (from top to bottom) pseudobreakups, small-oval, medium-oval and large-oval substorms. The IMF sign distributions before and after the events are not presented here, as they do not reveal any larger changes (despite a decrease of southward IMF B_z cases around large-oval substorm onsets). There is a clear increase of southward IMF cases from pseudobreakups, small-oval, medium-oval to large-oval substorms. More than two-thirds of the pseudobreakups appear during northward IMF Bz. Even small-oval substorms have a majority of northward IMF cases. Medium-oval and large-oval substorms appear mainly during southward IMF. The latter occur nearly exclusively for southward IMF.

In Figure 3 the distribution of the IMF B_z values for 12 different ranges are shown. The horizontal lines mark the average IMF B_z distribution during the statistical time period, they indicate a Gaussian distribution slightly displaced towards weakly positive Bz. The average IMF B_z value shifts from weakly positive to strongly negative between pseudobreakups, small-oval, medium-oval and large-oval substorms. The IMF clock angle distribution is not shown here. It is similar to the IMF B_z distribution because of a nearly average IMF B_y distribution for all types. The number of cases with negative IMF B_x (positive IMF B_y) in Figure 2 decreases between small-oval, medium-oval and large-oval substorms.

The IMF B_x and B_y sign distribution is coupled to the strength and sign of IMF B_z. This is shown in Table 1. There, the distributions of the IMF B_x and B_y signs during the statistical time period are shown for four IMF B_z intervals (the interval ranges are chosen such that the IMF B_z values of each interval appear 25 % of the statistical time period) During strongly northward IMF, the IMF B_x (By) component is most of the time negative (positive). With decreasing IMF Bz, the distribution changes towards less often negative (positive) IMF B_x (By) values. From Figure 1 it is known that substorms with increasing oval-size occur typically for decreasing IMF B_z values. These results show, that IMF B_x and B_y sign distribution of the different substorm types are coupled to the IMF B_z values typical for each type.

The dependence of substorms and pseudobreakups on IMF magnitude, solar wind velocity, density and the AE index

Figure 4 shows the distribution of the IMF magnitude (the absolute value of the IMF, averaged over the event lifetime), the solar wind speed and the solar wind ion density. The plots are done in the same way as Figure 3, except that the solar wind parameters are now divided into four intervals. The range of each interval is chosen such that the solar wind parameter has values within one interval during 25 % of the statistical time period. The plots in Figure 4 all show a similar shift in the distribution between pseudobreakups, small-oval, medium-oval and large-oval substorms. Most pseudobreakups occur for IMF magnitudes, solar wind velocity and density values that are lower than the average distribution during the statistical time period. With increasing oval size, the number of substorms having high IMF, velocity and density values increases.

The distribution plots of the kinetic energy flux (approximated by $n_i v^3$) and the magnetic energy flux (approximated by $vB^2/2\mu_0$) are not shown here. They reveal an even more pronounced shift between many cases with low values to many cases with high values from pseudobreakups to large-oval substorms.

In Figure 5, the distribution of the epsilon parameter is compared to the AE index distribution. The expected similarity of the AE and epsilon distribution plots for each substorm type is confirmed. There is an extremely clear shift of the epsilon distribution peak from very low values for pseudobreakups to very high values for large-oval substorms. A similar shift occurs in the AE index plots. Even for pseudobreakups a similar distribution is found in both parameters, although the localized and high-latitude position of pseudobreakups could have been expected to result in a too low AE index value.

Solar wind dependence of the longitudinal onset position

The division into events with dawn, midnight and dusk onsets for pseudobreakups and substorms shows that the longitudinal onset location of pseudobreakups does not differ from substorms regarding occurrence frequency and IMF dependence. The majority of substorms (pseudobreakups) appears on the dusk side, 12%(19%) occur at midnight, 12%(15%) at the dawn side of the oval. As expected from previous reports [e.g., *Liou et al.*, 2001], a clear majority of dawnside substorms and pseudobreakups appears during negative IMF By, midnight onset events show an average IMF B_y sign distribution while dusk onset events occur more often during positive IMF By. The statistical distribution of all other solar wind parameters reveals no correlation with the MLT onset location.

Solar wind conditions during non-substorm times

Having identified every substorm-like activity on the UV images, it is possible to obtain the solar wind parameter distributions during non-substorm times. It is found that during non-substorm times the IMF is predominantly northward. All other solar wind parameter distributions are only marginally shifted towards lower values. During many of the non-substorm intervals polar auroral arcs occur. Polar arcs have a high occurrence probability during northward IMF, large IMF magnitudes and a high solar wind speed [*Kullen et al.*, 2002].

Subtracting all polar arc events (identified as small splits and clear polar arc events in *Kullen et al.* [2002]) from the non-substorm intervals, the solar wind parameter distribution peaks shift clearly to lower values. This is shown in Figure 6, where the solar wind parameter distributions are given for time intervals during which the auroral oval is in its ground state. The plots are produced for the same parameters and interval ranges as in Figures 3-5. The non-activity intervals are defined as those periods of time where neither substorm activity (pseudobreakups, substorms, unclear substorm events) nor polar arcs (clear polar arcs, small splits, unclear polar arc events) are visible on the UV images during at least two hours. Periods where the imager shows only a small part of the auroral oval are subtracted (2 h before and after each period where no UV images are available), to exclude events missed due to a too small field-of-view. The solar wind conditions during intervals when the auroral oval is in the ground state, are comparable to the conditions for pseudobreakups (top plots in Figures 3-5). IMF B_z is weakly positive, all other parameters have typically low (IMF magnitude and solar wind density) or very low values (solar wind velocity, epsilon parameter). The small difference in the distributions for pseudobreakups and no-activity intervals may be caused by the method of selecting no-activity intervals. Depending on how small no-activity intervals are counted as events, the solar wind parameter distributions change slightly.

Single, growth phase and recovery phase pseudobreakups

The division into single, growth phase and recovery phase pseudobreakups is based on the observation that these frequently occur during quiet times, just before substorm onset or at the very end of a substorm recovery phase. The three pseudobreakup types can be distinguished in the overview plot of Figure 8. It is a time-sequence plot for one month, where all pseudobreakups identified in Polar UVI images are overlaid on the AE index and IMF B_z curves. The IMF B_z values are shifted one hour to account for the propagation time between ACE and Earth. The gray shaded bars mark the times where no UV images are available. Figure 8 illustrates the results of the AE distribution plots in Figure 5. A majority of pseudobreakups appears during times of small or no substorm activity with very low AE values. They may develop just before or just after periods of recurrent strong substorms, but not within such sequences. A clear example is the 24-hour period of enhanced AE index values during December 23-24 where several substorm onsets can be distinguished. The last pseudobreakup appears just before the onset of the first substorm within the cycle, the next pseudobreakup appears when the substorm cycle has nearly reached its end, during the recovery phase of the last substorm.

The spatial evolution of single, growth phase and recovery pseudobreakups

The Polar UV images reveal systematic differences in the auroral precipitation pattern between the different pseudobreakup types. About 80 percent of the single pseudobreakups appear in the main oval, the remaining events occur near the poleward oval boundary or develop a bulge that reaches into the polar cap. Single pseudobreakups often appear when the oval is thick, while growth phase pseudobreakups most of the time occur on a thin oval. Hence, it is in most cases not possible to determine whether growth phase pseudobreakups appear near the poleward or near the equatorward oval boundary (due to the limited resolution of Polar UVI). An examination of the longitudinal onset location or growth phase pseudobreakups reveals that only 42 percent appear (approximately) at the same place as the following substorm onset. Those pseudobreakups that have a deviating onset location, appear mainly duskward (25%) and/or poleward (35%) of the onset. Only in a few cases the onset is dawnward or equatorward of the following substorm onset. Single and growth phase pseudobreakups can occur as localized spots as well as elongated brightenings, with an extension of several hours MLT. Fluctuations and a motion along the oval are often found for single pseudobreakups with a long life time. These features are more rarely observed for growth phase pseudobreakups, because of their short lifetime (by definition shorter than 30 minutes). Over 80 percent of the growth phase pseudobreakups appear for less than 15 minutes.

The spatial evolution of recovery phase pseudobreakups deviates strongly from the other pseudobreakup types. They occur nearly exclusively at the poleward oval boundary at the very end of an active substorm recovery. In most cases, the polar cap has reduced its size considerably during the substorm which precedes a recovery phase pseudobreakup. The oval becomes thick and the poleward boundary is found on very high latitudes. The nightside part of the oval is typically very active with auroral streamers, multiple PBI's and bulges that extend into the polar cap. Often, during the last part of substorm recovery, the poleward boundary remains at high latitudes while the main oval between poleward and equatorward boundary fades away, so that a double-oval like structure evolves. In some cases, the activity along the poleward oval boundary reduces to one localized spot while the oval returns to the ground state. Such an event is here defined as recovery phase pseudobreakup. Many recovery pseudobreakups are disconnected from the main oval during a major part of their lifetime, but merge at the end with the main oval. Only for very few events, the recovery phase pseudobreakup appears on a bulge that is connected to the main oval. In such cases, the recovery is less active and no double-oval structure has developed.

Many pseudobreakups occur at the same time as polar auroral arcs are visible in the polar cap. About half of the recovery phase pseudobreakups, one third of the single pseudobreakups and about one fourth of the growth phase pseudobreakups appear in connection with polar arcs. A pseudobreakup is often found near or at the oval connection point of the arc (as recently reported by *Hubert et al.*, [2004]). Sometimes the brightening spreads partly along the arc. Most polar arcs occurring simultaneously with pseudobreakups are small arcs near the main oval boundary.

Most pseudobreakups occur when the oval is very small. Two-thirds are small-oval pseudobreakups (one third occurs for an extremely contracted oval with the equatorward oval boundary at 66 Cglat or higher) and one third are medium-oval pseudobreakups. In only 6 cases, the oval is large.

Table 2 gives information about the type of substorm that appears just before or after a pseudobreakup event takes place. All substorms are counted as events where one or more pseudobreakups occur within one hour before (left column) or after the substorm (right column). The result is given in percentage of substorm type and as number of pseudobreakup events. The majority of substorms that are preceded or followed by a pseudobreakup are small-oval or medium-oval substorms. Pseudobreakups occur also often after substorms during which the oval has contracted. It is extremely unusual that pseudobreakups appear before large-oval or after expanding-oval substorms. This means, the probability that a pseudobreakup develops just before (after) a substorm is high, when the oval is small at substorm onset (during recovery).

The influence of solar wind parameters on single, growth phase and recovery phase pseudobreakups

In Figures 8 to 10, distribution plots of the IMF sign, the IMF B_z value, the epsilon parameter and the AE index are shown for the different pseudobreakup types. Figures 8 and 9 are produced in the same way as Figures 1 and 2.

The IMF B_z sign distribution in Figure 8 varies strongly between the different types and in time. For a large majority of single pseudobreakups, the IMF is northward before, during and after the event. Growth phase pseudobreakups appear an hour after the B_z distribution has changed from a majority of northward to a majority of southward cases. An equal IMF B_z sign distribution appears the hours after the events. For recovery phase pseudobreakups the opposite shift appears in the IMF B_z sign distribution. It takes several hours until a distribution of mainly southward IMF cases changes towards mainly northward cases during the events. After the events, there is only a small majority of northward IMF cases left. The IMF B_x and B_y sign distributions in Figure 8 show an only small deviation from the average sign distribution. The small difference in the IMF B_x and B_y sign distribution between single and recovery phase pseudobreakups compared with the growth phase pseudobreakups may be explained by the small distribution shift between times with weakly northward and weakly southward IMF (as shown in Table 1). As shown in the IMF B_z distribution plots in Figure 9, single and recovery phase pseudobreakups appear during weakly northward, growth phase pseudobreakups during weakly southward IMF. Hence, even for pseudobreakups, the IMF B_x and B_y sign distributions are coupled to the IMF B_z value typical for each type.

From the IMF B_z sign distribution in Figure 8 it cannot be concluded that in each single case an IMF B_z southturn (northturn) takes place before a growth phase (recovery phase) pseudobreakup appears. Table 3 gives the percentage of cases which contain at least one IMF B_z southturn or northturn within one hour before onset (second column) and within one hour after onset (third column). The table shows the same tendency as the IMF B_z sign distribution plots in Figure 8. There are clearly less single pseudobreakups connected with IMF B_z sign changes than growth phase and recovery phase pseudobreakups. Most growth phase pseudobreakups appear after an IMF B_z southturn and are followed by an IMF B_z northturn. The opposite sign reversal appears before and after recovery phase pseudobreakups.

The IMF magnitude, solar wind velocity and density distribution plots for the different pseudobreakup types are not shown here. There are only minor differences seen between the distributions. Single pseudobreakups have marginally lower IMF magnitude and solar wind velocity values than the two other types, recovery phase pseudobreakups appear more often for low density values.

In Figure 10, the epsilon parameter and the AE index distributions are shown at the event start (left black bar), during (right black bar) and the hours before (gray bars) and after (white bars) the events. Epsilon parameter and AE index have a similar distribution for single and recovery phase pseudobreakups: The majority of the events occurs for very low AE and epsilon values. The maximum number of events with lowest values occurs during the events, before and after the event there are slightly more cases with higher values. For growth phase pseudobreakups the AE and epsilon distributions deviate from each other. For most growth phase pseudobreakups the epsilon parameter has average values while the AE index is low. Also the distribution change in time is different. The epsilon distribution has a small peak at highest values during the event while the AE index has in most cases lowest values during the events.

The influence of solar wind parameters on poleward and middle pseudobreakups

Due to the low image resolution of Polar UVI, the results for poleward (122 events) and middle pseudobreakups (208 events) have to be treated with care. The high number of middle pseudobreakups shows, that in most cases the oval is thin and the location of a pseudobreakup within the oval can not be identified. In 16 percent of all middle pseudobreakups, the brightening was slightly polewardly displaced (but not clear enough to be counted as poleward pseudobreakup). From previous work it can be assumed that most growth phase pseudobreakups do not appear near the poleward boundary. Thus, there is a high probability that the group of middle pseudobreakups contains both, poleward and equatorward events.

Poleward pseudobreakups are in a majority recovery pseudobreakups. (21, 11 and 94 percent of the single, growth phase and recovery phase pseudobreakups develop at the poleward oval boundary). The group of middle pseudobreakups consists mainly of single pseudobreakups. The few pseudobreakups where a clear equatorward onset location could be identified consist of 14 single and 5 growth phase pseudobreakups. They appear all on the equatorward branch of a double-oval with no visible particle precipitation between the two parts. In 5 of these cases a second pseudobreakup appears simultaneously at the poleward oval part. All of these are included into the group of middle pseudobreakups.

The pseudobreakup onset location seems to be independent on solar wind parameters and on the oval size. In Figure 11a, the distribution of poleward and middle pseudobreakups with respect to the location of the equatorward oval boundary are given. The distributions of both groups are very similar, they appear for a broad range of oval sizes. For none of the solar wind parameter distributions, a clear difference between poleward and middle pseudobreakups is found. The largest difference is found for in the IMF B_z distributions, shown in Figure 11b. Both pseudobreakup types occur in a majority during weakly northward IMF, but poleward pseudobreakups appear slightly more often for higher IMF Bz values.

Discussion

In contrast to comparable studies, all substorm-like activities are included in the present work, from extremely weak localized brightenings to large storm-time substorms. The complete coverage of all substorm activities appearing during the statistical time period of 3 months makes it possible to calculate their occurrence frequency, compare the solar wind conditions during substorms with non-substorm times and investigate the place of pseudobreakups within substorm cycles. The high number of identified events allows to determine the typical solar wind conditions for each substorm and pseudobreakup type.

The drawback of this method is, that both the group of substorms and the group of pseudobreakups contain substorm-like activities that may be classified differently. As defined here, substorms include even SMC events, and stormtime expansions without clear equatorward onset. The group of pseudobreakups includes all auroral activations that take place outside substorm expansion and recovery, independent whether they appear near the poleward or equatorward oval boundary. The reason why (non-substorm) PBI's are not counted as an own group lies in the limited image resolution of Polar UVI. Small auroral intensifications occur often when the oval is rather thin and the brightening appears on UVI as broad as the oval itself and the exact onset position can not be determined.

Table 4 summarizes the characteristic solar wind conditions during substorms and pseudobreakups, during times the auroral oval is in its ground state and during polar auroral arcs. The results are derived from the present study and from the findings by *Kullen et al.* [2002]. Treating all substorms as one group (small-, medium-, large-, expanding-, shrinking-oval substorms) results in a solar wind parameter distribution with a small majority of southward IMF cases and a nearly average distribution of all other solar wind parameters. The solar wind conditions during intervals when the auroral oval is in the ground state (neither substorm activity nor polar arcs) are comparable to the conditions for pseudobreakups. IMF B_z is weakly positive, all other parameters have typically low values. A major difference between solar wind conditions during pseudobreakups and no-activity times has not been found. This suggests that there is always enough energy available for the development of a pseudobreakup. The solar wind conditions typical for substorms clearly deviate from those for polar arcs. Most of the polar arcs appear during solar wind conditions with a high energy flux. However, the majority of polar arcs is connected to only average epsilon values due to the predominantly northward IMF conditions of polar arcs. Our interpretation is, that substorms need less solar wind energy than polar arcs due to the better energy coupling for southward than for northward IMF.

IMF dependence of substorms

The IMF characteristics found for substorm are in agreement with previous findings (Figures 1-5a). Substorms occur predominantly during southward IMF with a negative B_x and a positive By component [*Rostoker*, 1968]. The IMF B_x and B_y sign distributions during substorms correspond to the average IMF B_x and B_y distributions, taken over several years [*Wilcox and Ness*, 1965]. The dependence of substorms on IMF B_z changes is reproduced in our study as well. The shift in the IMF B_z sign distribution of Figure 1 indicates the expected IMF B_z decrease (increase) for expanding- and shrinking-oval substorms. Even the hour long time delay between IMF southturn and substorm onset (until enough energy is stored in the tail) as well as the immediate start of a substorm after an IMF B_z northturn (triggered by a sudden energy release due to the closure of the magnetosphere) can be distinguished in the distribution plots. This shows that large-scale changes in the solar wind that have an effect on the occurrence of an auroral phenomenon can be discovered by studying hourly averaged solar wind parameter distributions before and after the events, as done here.

The main difference between our statistical results for substorms and results of other studies lies in the high number of substorms appearing during predominantly northward IMF. In most of the northward IMF cases, IMF B_y is larger than or equal to IMF B_z. The 44 % of northward IMF substorms, found in our study, include cases with purely northward IMF as well as cases, where the IMF turns northward during the event. In our study, 28 % of all substorms (28 % pseudobreakups) were found to have positive IMF B_z during at least 20 minutes before and after the onset. *Hsu and McPherron* [2003] found only 10 % of such cases. Similar numbers have been reported even in other studies. The higher number of northward IMF cases in our statistical study as compared to *Hsu and McPherron* [2003] and others is probably connected to the different substorm definitions in the studies. In our statistical study we count any auroral breakup that leads to a visible auroral expansion as substorm, even those that are very weak or on very high latitudes (no clear AE enhancement), while others have as additional requirement a sharp AL decrease and/or Pi2 pulsations.

The large number of substorms during northward IMF shows that an energy transfer into the magnetotail is very well possible during such conditions as long as IMF B_z is small compared to the IMF B_y component. This basically confirms the validity of the epsilon parameter [*Akasofu*, 1980] and similar energy coupling parameters that contain the factor $sin^x(\theta/2)$ ($x = 1, 2$ or 4). This is difficult to understand, as the classical substorm model requires dayside reconnection to obtain an energy transfer into the magnetosphere, which is assumed to take place only during southward IMF. During northward IMF, reconnection appears at the high-latitude lobes, prohibiting the addition of open flux on the tail. Based on observations, *Baumjohann* [1996] proposed that the NENL model may hold only for storm-time substorms while quiet time substorms may be connected to lobe reconnection. However, *McPherron and Hsu* [2002], repeating the study for a larger dataset, found that there was no difference between the two substorm types. They concluded that all substorms must have the same type of underlying mechanism. We see several possible scenarios that may explain the high number of substorms occurring during northward IMF. Small-scale spatial variations of the IMF during conditions with weakly positive IMF B_z (as typical for small-oval substorms and pseudobreakups) may lead to small regions of southward IMF. These could cause local dayside reconnections through which an enhanced energy transfer is possible. Another explanation is, that it takes several hours until the magnetosphere is emptied from all energy that is available for substorm related processes, so that long after a northturn internally triggered substorms may still occur.

Pseudobreakups in comparison with substorms

The method of classifying substorms via the average oval size during the substorm lifetime (approximated by the position of the equatorward oval boundary at midnight) is shown to work well. As can be seen from the AE distribution plots in Figure 5b, the groups of small-oval, medium-oval and large-oval substorms consist mainly of weak, moderate and strong substorms, as expected by the close relation between substorm strength and oval size [*Feldstein and Starkov*, 1967]. This substorm classification allows to compare the solar wind parameter distributions for pseudobreakups with those for substorms of increasing strength.

The solar wind parameter distribution for pseudobreakups reveals that these occur predominantly during low IMF magnitude, solar wind density and velocity. In most cases, IMF B_z has weakly positive values (0-1.5 nT), which confirms the results by *Zhou and Tsurutani* [2001] of near zero IMF Bz during pseudobreakups. The observed systematic shift from low solar wind parameter values (weakly positive IMF Bz) for pseudobreakups to increasingly higher values (stronger negative IMF Bz) for substorms of increasing strength supports the scenario proposed by *Nakamura et al.* [1994] and others, that pseudobreakups are not fundamentally different from substorms, but the weakest possible type that occurs when the solar wind energy transfer is not high enough for a substorm to occur. These results fit well to the numerous observations that did not reveal any significant difference in the ionospheric and magnetospheric signatures of pseudobreakups, PBI's and substorm breakup, other then location of the tail source region [*Sergeev et al.*, 1996b].

Onset location of substorms and pseudobreakups

Our statistical results confirm the dependence of substorm onset location on IMF magnitude and IMF B_z (latitudinal onset location) and on IMF B_y (longitudinal onset location), which have been reported by *Liou et al.* [2001] and others. The latitudinal onset position can be approximated by the equatorward UV oval boundary, because substorm onset appears at a fixed distance of 3-4 degrees from this boundary [*Gerard et al.*, 2004]. Thus, the results of Figures 3 and 4a for substorms of different oval sizes can be interpreted as results for substorms with different onset locations. The more equatorward onset region during strong and southward IMF [*Holzworth and Meng*, 1984] is expected from the more earthward location of the inner plasma sheet boundary during enhanced convection [*Lyons et al.*, 1999]. Substorms with dawn onset are more common during dawnward IMF B_y, dusk onsets occur more often for duskward IMF B_y. This IMF B_y dependence can be explained by the IMF B_y induced dawn-duskward bending of magnetospheric B-field lines [e.g., *Kaymaz et al.*, 1994] which causes for dawnward (duskward) IMF B_y a clockwise (anti-clockwise) displacement of the closed field line footprints in the northern ionosphere [*Kullen and Blomberg*, 1996]. The low number of dawn onsets (15%) may be related to the low appearance rate of dawnward IMF B_y during the statistical time period. The occurrence frequency of dawn onsets, found in this statistics, is comparable to 10% dawn onsets, found by *Liou et al.* [2001].

As for substorm breakup, the MLT position of pseudobreakups is controlled by IMF B_y. Most dawn and dusk pseudobreakups occur during dawnward and duskward IMF B_y, respectively. In opposite to substorm breakup, there is no IMF Bz dependence found for the pseudobreakup position with respect to the oval boundaries. Due to the difficulty in determining the onset location on a thin oval, the results from a comparison between middle (thin oval) pseudobreakups and poleward pseudobreakups in Figure 11 have to be treated with care. However, the results for poleward pseudobreakups can be trusted.

In opposite to what could have been expected, far from all poleward pseudobreakups occur during northward IMF or on a highly contracted oval (Figure 11). This indicates that the pseudobreakup location within the oval is not directly controlled by IMF Bz. Instead, a clear correlation between pseudobreakup location and substorm phase is found. Nearly all recovery phase pseudobreakups appear at the poleward oval boundary. From Polar UVI, the onset position of growth phase pseudobreakups cannot be determined exactly (the majority are middle pseudobreakups), but from other studies it is known that growth phase pseudobreakups do not appear near the poleward oval boundary. This fits to the scenario described by *Sergeev et al.* [1996b], where the substorm phase defines the large-scale structure of the magnetosphere and even the source region of small auroral activations. Substorm onset appears on the most equatorward arc, followed by a poleward motion of the intensification region. During expansion and recovery, auroral intensifications (PBI's) start near the poleward boundary.

In our study, no significant difference in the solar wind parameter distributions have been found between the group of poleward and middle pseudobreakups. From previous work it is known that pseudobreakups and PBI's have nearly identical ionospheric [*Rostoker*, 1998] and magnetospheric signatures. *Nakamura et al.* [2001] showed, that pseudobreakups, PBI's and auroral streamers are all associated with BBF's in the magnetotail, the difference being the more tailward source region of BBF's connected to recovery intensifications. As long as no significant difference in any of the magnetospheric signatures or solar wind conditions are found, it cannot be ruled out that poleward pseudobreakups (PBI's) and non-poleward pseudobreakups have the same formation mechanism, as proposed by *Sergeev et al.* [1996b].

IMF dependence of single, growth phase and recovery pseudobreakups

Single pseudobreakups occur during quiet times with extremely low positive IMF B_z values. The lack of large changes in the IMF sign distribution before, during and after single pseudobreakups in Figure 8 and the low rate of IMF B_z sign changes in Table 3 show, that the majority of these are not systematically connected to large-scale IMF changes. The detection of possible pseudobreakup triggers is not part of this study. However, we found a few single pseudobreakup events where IMF and solar wind can be excluded as triggers. During February 20, 22 and 26, nearly constant solar wind conditions last during many hours. After 8 hours (5 hours) of completely constant IMF with a weakly northward direction a weak pseudobreakup appears. The results indicate that single pseudobreakups are just the smallest type of substorms appearing during weakly northward IMF, possibly caused by an internal instability. The high rate of hybrid cases between single pseudobreakups and weak substorms strengthens the view that there is a gradual shift between what can be interpreted as a substorm and single pseudobreakups.

Figure 8, Figure 9 and Table 3 give a view on the typical IMF conditions around growth phase pseudobreakups. They appear about an hour after IMF B_z has changed from positive to weakly negative values. An IMF northturn occurs during or soon after the onset of the growth phase pseudobreakup. Growth phase pseudobreakups are followed by small or medium-oval substorms that appear during weakly northward IMF (Table 2). The results are in agreement with previous work. Growth phase pseudobreakup events have been reported to appear during [*Pulkkinen et al.* 1998; *Rostoker* 1998] or at the end of a southward IMF period [*Voronkov et al.*, 2003; *Partamies et al.*, 2003].

The IMF B_z excursion towards weakly southward IMF before the onset is related to a small epsilon maximum during growth phase pseudobreakups (Figure 10a). Studying solar wind parameter time series for each of the growth phase pseudobreakups reveals, that they often start during or just after a small epsilon maximum, that lasted for about an hour. The average epsilon value during the hour before the pseudobreakup lies in 49% of the cases slightly above 100 GW. This epsilon value has been proposed by *Akasofu* [1980] to be the threshold value for substorms to break out. (The corresponding numbers for single pseudobreakups, recovery pseudobreakups and all substorms are 13 %, 29 % and 65 %). This means, for half of the growth phase pseudobreakups the solar wind energy input was high enough to trigger a real substorm onset. The global expansion of a growth phase pseudobreakup may be prevented by the instantaneous decrease of the energy transfer into the tail, as indicated by the decreasing epsilon value. The following, rather small substorm starts probably due to a lower energy threshold for IMF B_z triggered substorms, as suggested by *Yahnin et al.* [1983]. Such a mechanism has been proposed by *Partamies et al.* [2003], who studied a growth phase pseudobreakup with nearly identical solar wind characteristics as found in our statistical study.

Recovery phase pseudobreakups appear when the energy transfer to the magnetosphere is very low, about 1-2 hours after an IMF northturn. The IMF change takes place during the preceding substorm and explains the strong contraction of the polar cap boundary. It is caused by the accumulation of closed field lines when the dayside reconnection vanishes due to the IMF northturn [*Pytte et al.*, 1978]. Multiple expansion phase and recovery phase PBI's are quite common during such substorms. Many recovery pseudobreakup resembles recovery PBI's, as both appear at the polewardly displaced oval boundary and often involve an equatorward motion at the end of their lifetime. Why and how the poleward oval part remains active on a single spot (as is the case for most recovery phase pseudobreakups) while the main oval retreats to its ground state, remains to be shown.

The place of pseudobreakups within substorm cycles

The schematic in Figure 12 summarizes the results of Figures 7 to 9. It illustrates how pseudobreakups are related to IMF B_z and large substorm cycles. Pseudobreakups seem to appear randomly during quiet times as long as the IMF B_z component is weakly positive and the solar wind energy is low. At the end of a 30-60 minutes long IMF excursions towards weakly southward IMF, pseudobreakups may appear just before a rather small substorm starts. In cases the IMF becomes strongly southward during a prolonged period of time, many strong substorms occur after each other. This period is devoid of pseudobreakups. An IMF northturn (at substorm onset or during the substorm) ends this cycle. During the last substorm, the poleward oval boundary contracts considerably due to the IMF B_z increase, and a very active recovery phase ends with a recovery pseudobreakup. An observational paper by *Voronkov et al.* [2003] contains a case study with an IMF B_z curve similar to Figure 12. The corresponding substorm sequence consists of growth phase pseudobreakups two substorms and recovery PBI's during the later substorm as expected from our statistical results.

Possible tail configuration for single, growth phase and recovery pseudobreakups

Despite the differences between single, growth phase and recovery phase pseudobreakups, all three types have several features in common. They occur typically during times when the energy flux in the solar wind is low and IMF B_z is very small. Another common characteristics is a long tailward extension of the closed field line region during the events.

Several MHD simulations show that the length of the closed field line region is inversely proportional to positive IMF Bz [e.g., *Gombosi et al.*, 1998]. An extension of the closed field line region to over 100 R_E and an strong magnetic field line stretching in the inner tail is observed for weakly northward IMF or during the first hour after an IMF B_z northturn, which are the typical conditions during single and recovery phase pseudobreakups, respectively. The MHD results are supported by observations of earthward BBF's that appear in distant tail regions beyond 100 R_E predominantly during northward or near zero IMF B_z [*Troshichev et al.*, 1999].

The tailward stretching of magnetic field lines during the growth phase is well-known. It reaches its maximum just before substorm onset. MHD results by *Pulkkinen et al.* [1998] indicate, that even if a NENL forms already during a growth phase pseudobreakup, the large-scale near-Earth tail topology does not change and consists of strongly stretched magnetic field lines, connected to an extremely thin plasma sheet. The pseudobreakup in the simulation maps to this region.

The tailward retreat of the plasma sheet and closed field line region during recovery becomes extreme, in case a double-oval structure evolves. The old, tailward closed field line part (poleward oval part) becomes more and more separated from the new, earthward closed field line part (equatorward oval part). Recovery pseudobreakups, appearing at the fading poleward oval part, are connected to the most distant closed field lines and plasma sheet region.

How the described large-scale magnetotail topologies for the different pseudobreakup types could affect the occurrence of small auroral intensifications, remains to be shown.

Summary

In this study, a statistical analysis of substorm activity is performed, based on Polar UVI images and ACE solar wind data. The solar wind parameters of large-scale substorm-activity (storm-time expansions, SMC's, substorms) are compared to single, localized auroral intensifications (including PBI's outside substorm expansion and recovery), here referred to as pseudobreakups.

The data show that there is a gradual increase of typical values for IMF magnitude, solar wind velocity and density, and a shift from weakly northward to strongly southward IMF B_z between pseudobreakups and substorms of increasing strength. These results confirm the scenario developed from detailed single case studies that pseudobreakups are not fundamentally different from substorms, but the weakest possible type that occurs when not much energy is available in the solar wind and the coupling between solar wind and magnetosphere is low.

Pseudobreakups may appear before the first or after the last substorm of a substorm cycle. Periods of recurrent strong substorms are devoid of pseudobreakups, probably because the solar wind energy input into the magnetosphere during such periods is too high for a pseudobreakup to occur.

Pseudobreakups occur as single events during quiet times, during substorm growth phase or at the end of the recovery phase. The IMF is weakly northward during most single and recovery phase pseudobreakups. Growth phase pseudobreakups appear mainly during weakly southward IMF. Solar wind characteristics and optical observations suggest that single pseudobreakups are the smallest possible type of substorms, occurring during quiet times. The appearance of growth phase pseudobreakups at the end of a period with slightly enhanced epsilon values, suggests that a decrease of the energy transfer into the tail quenches a further expansion of the breakup. Recovery phase pseudobreakups are a special type of single PBI occurring at the very end of those substorms which show a considerable contraction of the poleward oval boundary due to an IMF northturn. They constitute the last remaining signature of the former poleward oval boundary that has moved equatorward.

No clear dependence on solar wind parameters is found for the pseudobreakup location with respect to the oval boundaries. It cannot be excluded that this result is caused by the limited image resolution of Polar UVI, not allowing a proper distinction between poleward and equatorward cases. In case the results are correct, they indicate, that the onset location of pseudobreakups is stronger influenced by the nearest substorm phase (non-poleward onset during substorm growth phase, poleward onset at the end of substorm recovery) than directly by solar wind conditions. This issue remains an important task for future studies.

Acknowledgments. We are grateful to G. Parks for providing Polar UV data and M. Brittnacher for producing the UV image sheets. We also want to thank N. Ness at Bartol Research Institute, D.J. McComas at Los Alamos National Laboratory and the CDAWeb for providing ACE solar wind data. We would like to acknowledge the WDC-C2 Kyoto AE index service, the AE stations and the persons who derive the index for access to preliminary AE index data on the world wide web.

References

Aikio, A. T., V. A., Sergeev, M. A. Shukhtina, L. I. Vagina, V. Angelopoulos, and G. D. Reeves (1999), Characteristics of pseudobreakups and substorms observed in the ionosphere, at geosynchronous orbit, and in the midtail, *J. Geophys. Res., 104*, 12,263.

Akasofu, S.-I. (1964), The development of the auroral substorm, *Planet. Space Sci., 12*, 273.

Akasofu, S.-I. (1980), The solar wind-magnetosphere energy coupling and magnetospheric disturbances, *Planet. Space Sci., 28*, 495, 1980.

Amm, O., P. Janhunen, K. Kauristie, H. J. Opgenoorth, T. I. Pulkkinen, and A. Viljanen (2001), Mesoscale ionospheric electrodynamics observed with the MIRACLE network, 1. Analysis of a pseudobreakup spiral, *J. Geophys. Res., 106*, 24,675.

Angelopoulos, V. et al. (1994), Statistical characteristics of bursty bulk flow events, *J. Geophys. Res., 99*, 21,257.

Baker, D. N., A. J. Klimas, and D. V. Vassiliadis (1995), Energy transfer between the solar wind and the magnetosphere-ionosphere system, *J. Geomagn. Geoelectr., 47,* 1171.

Baker, D. N., et al., Timing of magnetic reconnection initiation during a global magnetospheric substorm onset (2002), *G. Res. Lett., 29*, 2190, doi:10.1029/2002GL015539.

Baumjohann, W. (1996), Substorms, storms and the near Earth tail, *J. Geomagn. Geoelectr., 48* 177.

Berkley, F. T., and Y. Kamide (1976), On the distribution of global auroras during intervals of magnetospheric quiet, *J. Geophys. Res., 81*, 4701.

Elvey, C. T., Problems of auroral morphology (1957), *Proc. Nat. Acad. Sci.*, Washington, 43, 63.

Feldstein, Y. I., and G. V. Starkov (1967), Dynamics of auroral belt and polar geomagnetic disturbances, *Planet. Space Sci., 15*, 209.

Fillingim, M. O., G. K. Parks, L. J. Chen, M. Brittnacher, G. A. Germany, J. F. Spann, D. Larson, and R. P. Lin (2000), Coincident POLAR/UVI and WIND observations of pseudobreakups, *Geophys. Res. Lett., 27*, 1379.

Fuller-Rowell, T. J. , and D. S. Evans (1987), Height-integrated Pedersen and Hall conductivity patterns inferred from the TIROS-NOAA satellite data, *J. Geophys. Res, 92*, 7606.

Gerard, J.-C., B. Hubert, A. Gerard, and M. Meurant (2004), Solar wind control of auroral substorm onset locations observed with the IMAGE-FUV imagers, *J. Geophys. Res., 109*, A03208, doi:10.1029/2003JA010129.

Gombosi, T. I., D. L. DeZeeuw, R. M. Häberli, K. G. Powell, and P. Song (1998), The length of the magnetotail for northward IMF: Results of 3D MHD simulations, in *Physics of Space Plasmas,*, ed. T. Chang and J. R. Jasperse, vol. 15, p. 121, MIT Press, Cambridge.

Hardy, D., M. Gussenhoven, and E. Holeman (1985), A statistical model of auroral electron precipitation, *J. Geophys. Res., 90*, 4229.

Hardy, D. A., M. S. Gussenhoven, R. Raistrick, and W. J. McNeil (1987), Statistical and functional representations of the pattern of auroral energy flux, number flux and conductivity, *J. Geophys. Res. 92*, 12,275.

Henderson, M. G., J. S. Murphree, and J. M. Weygand (1996), Observations of auroral substorms occurring together with preexisting 'quiet time' auroral patterns, *J. Geophys. Res., 101*, 24,621.

Henderson, M. G., G. D. Reeves, and J. S. Murphy (1998), Are north-south structures an ionospheric manifestation of bursty bulk flows?, *Geophys. Res. Lett., 25*, 3737.

Holzworth, R. H., and C.-I. Meng (1984), Auroral boundary variations and the interplanetary magnetic field, *Planet. Space Sci., 32*, 25.

Hsu, T. S., and McPherron, R. L. (2003), Occurrence frequencies of IMF triggered and nontriggered substorms, *J. Geophys. Res., 108*, doi:10.1029/2002JA009442.

Hubert, B., J. C. Gerard, S. A. Fuselier, S. B. Mende, and J. L. Burch (2004), Proton precipitation during transpolar auroral events: observations with the IMAGE/FUV imagers, *J. Geophys. Res., 109*, doi:10.1029/2003JA010136.

Kamide, Y., P. D. Perreault, S.-I. Akasofu, and J. D. Winningham (1977), Dependence of substorm occurrence probability of the interplanetary magnetic field and on the size of the auroral oval, *J. Geophys. Res., 82,* 5521.

Kan, J. R., L. Zhu, and S.-I. Akasofu (1988), A theory of substorms: onset and subsidence, *J.*

Geophys. Res., 93, 5624.

Kaymaz, Z., G. L. Siscoe, J. G. Luhmann, R. P. Lepping, and Ch. T. Russell (1994), Interplanetary magnetic field control of magnetotail magnetic field geometry: IMP 8 observations, *J. Geophys. Res.*, *99*, 11,113.

Koskinen, H. E. J., R. E. Lopez, R. J. Pellinen, T. I. Pulkkinen, D. N. Baker, and T. Bosinger (1993), Pseudobreakup and substorm growth phase in the ionosphere and magnetosphere, *J. Geophys. Res., 98*, 5801.

Kullen, A., and L. G. Blomberg (1996), The influence of IMF B_y on the mapping between the Earth's magnetotail and its ionosphere, *Geophys. Res. Lett., 23*, 2561.

Kullen, A., M. Brittnacher, J. A. Cumnock, and L. G. Blomberg, Solar wind dependence of the occurrence and motion of polar auroral arcs: a statistical study (2002), *J. Geophys. Res., 107*, 1362, doi:10.1029/2002JA009245.

Liou, K., P. T. Newell, C.-I. Meng, M. Brittnacher, and G. Parks (2001), Characteristics of the solar wind controlled auroral emissions, *J. Geophys. Res., 106*, 5799.

Lui, A. T. Y. (1991), A synthesis of magnetospheric substorm models, *J. Geophys. Res., 96*, 1849.

Lui, A. T. Y.(1996), Current disruption in the Earth's magnetosphere: Observations and models, *J. Geophys. Res., 101*, 13,067.

Lui, A. T. Y., S.-I. Akasofu, E. W. Hones Jr., S. J. Bame, and C. E. McIlwain (1976), Observations of the plasma sheet during a contracted oval substorm in a prolonged quiet period, *J. Geophys. Res., 81*, 1415.

Lyons, L. R., G. T. Blanchard, J. C. Samson, J. M. Rouhoniemi, R. A. Greenwald, G. D. Reeves, and J. D. Scudder (1998), Near Earth plasma sheet penetration and geomagnetic disturbances in *New Perspectives on the Earth's magnetotail*, ed. A. Nishida, S. W. H. Cowley, and D. N. Baker, AGU, Washington, DC, 241.

Lyons, L. R., T. Nagai, G. T. Blanchard, J. C. Samson, T. Yamamoto, T. Mukai, A. Nishida, and S. Kokubun (1999), Association between Geotail plasma flows and auroral poleward boundary intensifications observed by CANOPUS photometers, *J. Geophys. Res., 104*, 4485.

McPherron, R. L. (1972), Substorm related changes in the geomagnetic tail: the growth phase, *Planet. Space Sci., 20*, 1521.

McPherron, R. L. (1991), Physical processes producing magnetospheric substorms and magnetic storms, in *Geomagnetism, vol. 4., ed. J. A. Jacobs*, Academic Press, San Diego, CA.

McPherron, R. L., and T. S. Hsu (2002), A comparison of substorms occurring during magnetic storms with those occurring during quiet times, *J. Geophys. Res., 107*, 1259.

Nakamura, M., D. N. Baker, T. Yamamoto, R. D. Belian, E. A. Bering III, J. R. Benbrook, and J. R. Theall (1994), Particle and field signatures during pseudobreakup and major expansion onset, *J. Geophys. Res., 99*, 207.

Nakamura, M., W. Baumjohann, M. Brittnacher, V. A. Sergeev, M. Kubyshkina, T. Mukai, and K. Liou (2001), Flow bursts and auroral activations: Onset timing and foot point location, *J. Geophys. Res., 106*, 10,777.

Ohtani, S. et al. (1993), A multi satellite study of a pseudo-substorm onset in the near-Earth magnetotail, *J. Geophys. Res., 98*, 19,355.

Partamies, N., O. Amm, K. Kauristie, T. I. Pulkkinen, and E. Tanskanen (2003), A pseudo-breakup observation: Localized current wedge across the postmidnight auroral oval. *J. Geophys. Res., 108*, doi:10.1029/2002JA009276.

Pellinen, R. J. , H. J. Opgenoorth, and T. I. Pulkkinen (1992), Substorm recovery phase: Relationship to next activation, in *Substorms 1, Eur. Space Agency Spec. Publ.*, 335.

Pulkkinen, T. I. (1996), Pseudobreakup or substorm ? in *Proceedings of the 3. international conference on substorms, May 13-17, 1996 Versailles, France, Eur. Space Agency Spec. Publ., SP-389,* 285.

Pulkkinen, T. I., D. N. Baker, M. Wiltberger, C. Goodrich, R. E. Lopez, and J. G. Lyon (1998), Pseudobreakup and substorm onset: Observations and MHD simulations compared, *J. Geophys. Res., 103*, 14,847.

Pytte, T., R. L. McPherron, M. Kivelson, E. W. Hones Jr., and H. I. West Jr. (1978), Plasma sheet recovery and the poleward leap of auroral zone activity, *J. Geophys. Res., 83*, 5256.

Rostoker, G. (1968), Relationship between the onset of a geomagnetic bay and the configuration of the interplanetary magnetic field, *Geophys. Res. Lett., 73*, 4382.

Rostoker, G. (1998), On the place of the pseudo-breakup in a magnetospheric substorm, *Geophys. Res. Lett., 25*, 217.

Rostoker, G. (2002), Identification of substorm expansive phase onset, *J. Geophys. Res., 107*, doi:10.1029/2001JA003504.

Rostoker, G., S.I. Akasofu, J. Foster, R. A. Greenwald, Y. Kamide, K. Kawasaki, A. T. Y. Lui, R. L. McPherron, and C. T. Russell (1980), Magnetospheric substorms - definitions and signatures *J. Geophys. Res., 85*, 1663.

Sergeev, V. A., A. G. Yahnin, R. A. Rakhmatulin, S. I. Solovjev, F. S. Mozer, D. J. Williams, and C. T. Russell (1986), Permanent flare activity in the magnetosphere during periods of low magnetic activity in the auroral zone, *Planet. Space Sci., 34*, 1169.

Sergeev, V. A., R. J. Pellinen, and T. I. Pulkkinen (1996a), Steady magnetospheric convection: A review of recent results, *Space Sci. Rev., 75*, 551.

Sergeev, V. A., T. I. Pulkkinen, and R. J. Pellinen (1996b), Coupled-mode scenario for the magnetospheric dynamics, *J. Geophys. Res., 101*, 13,047.

Snyder, C. W., M. Neugebauer, and U. R. Rao (1963), The solar wind velocity and its correlation with cosmic-ray variation and with solar and geomagnetic activity, *J. Geophys. Res., 68*, 6361.

Torr, M.R. et al. (1995), A far-ultraviolet imager for the international solar-terrestrial physics mission, *Space Sci. Rev., 71*, 329.

Troshichev, O. A., S. Kokubun, Y, Kamide, T. Mukai, and T. Yamamoto (1999), Fast earthward plasma flows observed in the mid/distant tail under quiet conditions: relation to substorms, *Geophys. Res. Lett., 26*, 643.

Voronkov,I. O., E. F. Donovan, and J. C. Samson (2003), Observations of the phases of the substorm, *J. Geophys. Res., 108*, 1073.

Wilcox J., and N. Ness (1965), Quasi-stationary corotating structure in the interplanetary medium, *J. Geophys. Res., 70*, 1233.

Yahnin, A. G., V. A. Sergeev, R. J. Pellinen, W. Baumjohann, K. U. Kailia, H. Ranta, J.

Kangas, and O. M. Raspopov (1983), Substorm time sequence and microstructure on 11 November 1976, *J. Geophys. Res., 53*, 182.

Zhou, X. Y., and B. T. Tsurutani (2001), Interplanetary shock triggering of nightside geomagnetic activity: Substorms, pseudobreakups, and quiescent events, *J. Geophys. Res., 106*, 18,957.

A. Kullen, Swedish Institute of Space Physics, Uppsala, Sweden (Anita.Kullen@irfu.se)

T. Karlsson, Alfvén Laboratory, Royal Institute of Technology, 10044 Stockholm, Sweden (tkarlsson@alfvenlab.kth.se)

Received ______________________

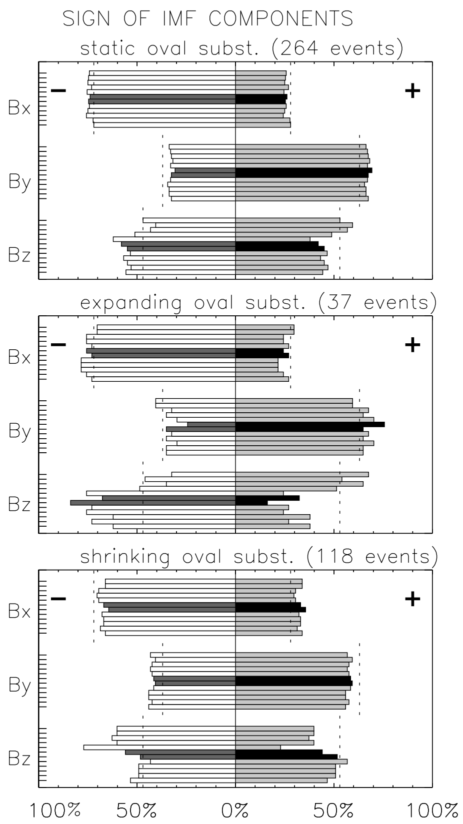
SIGN OF IMF COMPONENTS
static oval subst. (264 events)
expanding oval subst. (37 events)
shrinking oval subst. (118 events)
Bx
By
Bz
−
+
100%
50%
0%
50%
100%

Figure 1. The distribution of the sign of each IMF component as percentages of events for different substorm groups. Static-oval substorms are all substorms, where the equatorward oval boundary does not vary more than 1 degree in Cglat at 0 MLT, expanding-oval and shrinking-oval substorms are those where the equatorward boundary increases and decreases, respectively. The dotted lines give the distribution between positive and negative signs of each IMF component during the statistical time period. The gray bars above (below) the black bars show the distributions for the hourly averaged IMF component signs up to five hours before (after) the event. The top black bar shows the IMF component sign at the event start and the bottom black bar the average IMF component sign during the event.

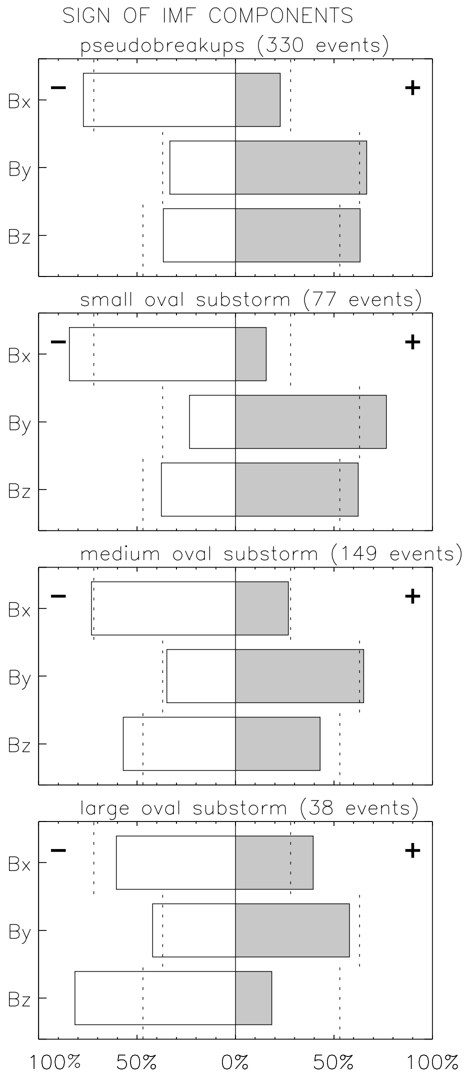
SIGN OF IMF COMPONENTS
pseudobreakups (330 events)
small oval substorm (77 events)
medium oval substorm (149 events)
large oval substorm (38 events)
Bx
By
Bz
−
+
100%
50%
0%
50%
100%

Figure 2. The distribution of the sign of each IMF component as percentages of events for pseudobreakups and static-oval substorms with the equatorward oval boundary at 64 Cglat or higher (small-oval substorm), between 60 and 64 Cglat (medium-oval substorm) and below 60 Cglat (large-oval substorm). The dotted lines give the distribution between positive and negative signs of each IMF component during the statistical time period. The bars show the distribution of the averaged IMF component sign during the substorms.

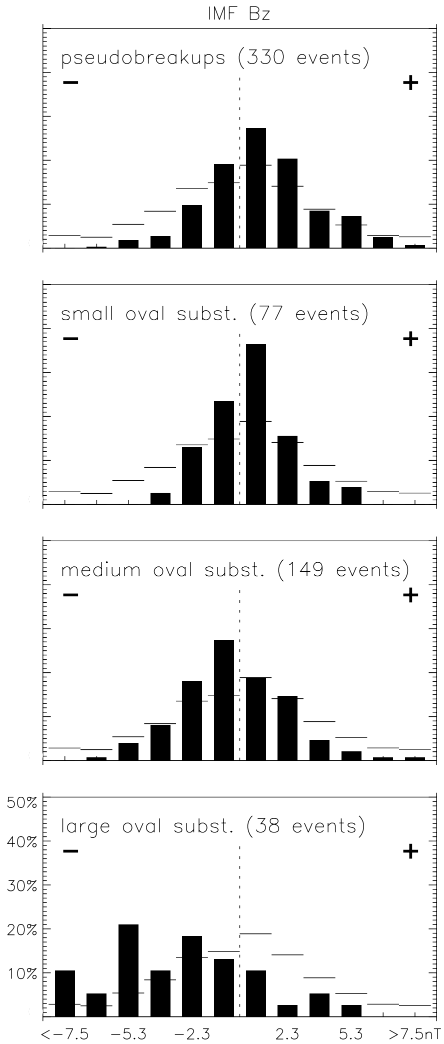
IMF Bz
pseudobreakups (330 events)
small oval subst. (77 events)
medium oval subst. (149 events)
large oval subst. (38 events)
−
+
50%
40%
30%
20%
10%
<−7.5
−5.3
−2.3
2.3
5.3
>7.5nT

Figure 3. The distribution of IMF B_z as percentages of events for pseudobreakups, small-oval, medium-oval and large-oval substorms. The distribution calculated for the average IMF B_z value during each substorm. The interval ranges between -7.5 and 7.5 nT have all the same width of 1.5 nT (0-1.5,1.5-3,3-4.5,...). The horizontal lines mark average IMF B_z distribution during the statistical time period.

Table 1. IMF B_x and B_y sign distributions for four equal IMF B_z intervals

IMF B_z:	< -2.3 nT	-2.3-0.2 nT	0.2-2.3 nT	> 2.3 nT
IMF $B_x < 0$	68 %	67 %	74 %	80 %
IMF $B_y > 0$	56 %	60 %	67 %	70 %

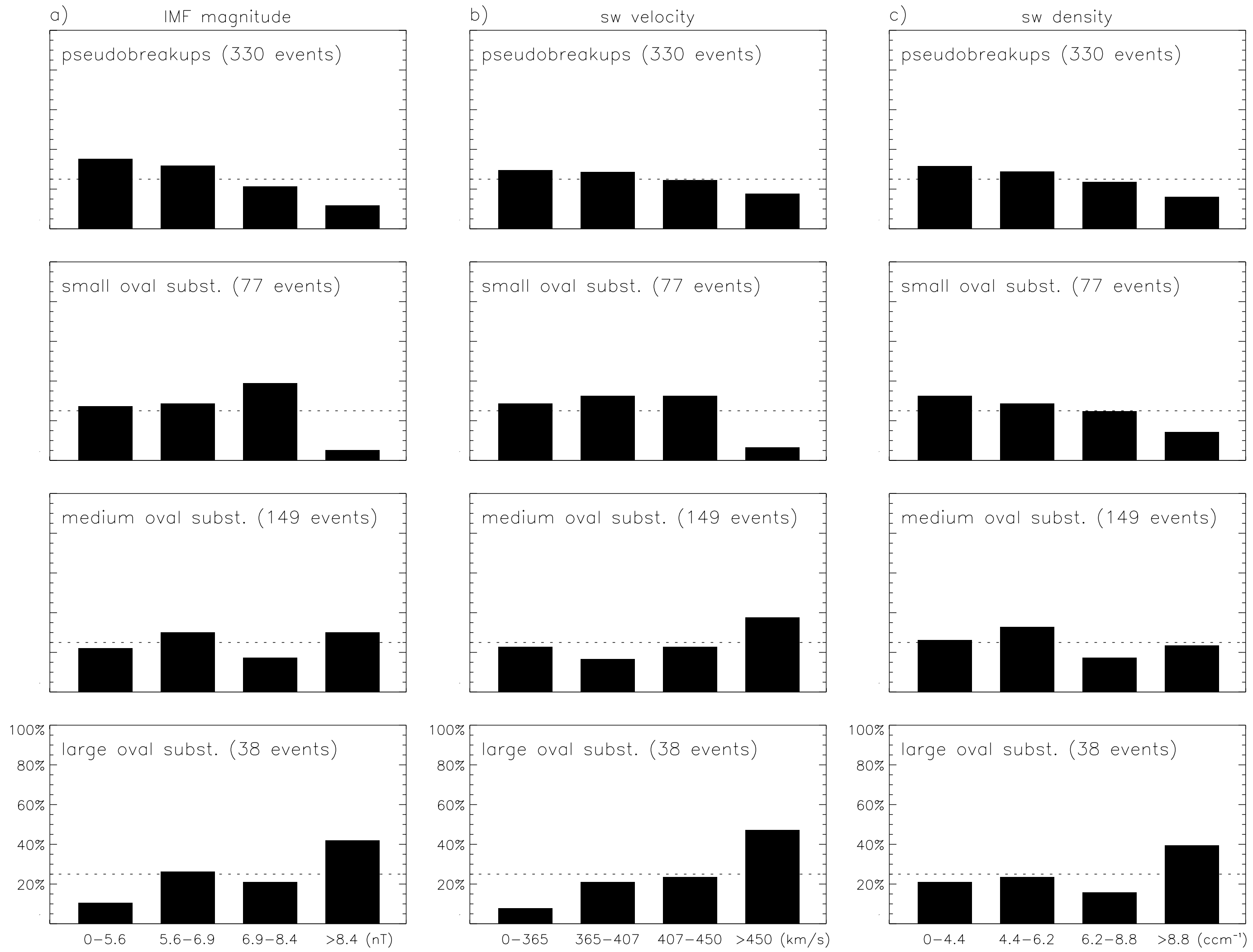
a) IMF magnitude
b) sw velocity
c) sw density
pseudobreakups (330 events)
small oval subst. (77 events)
medium oval subst. (149 events)
large oval subst. (38 events)
100%
80%
60%
40%
20%
0-5.6
5.6-6.9
6.9-8.4
>8.4 (nT)
0-365
365-407
407-450
>450 (km/s)
0-4.4
4.4-6.2
6.2-8.8
>8.8 (ccm⁻¹)

Figure 4. The distribution of a) IMF magnitude, b) solar wind velocity and c) solar wind density as percentages of polar arc events. The different magnitude ranges are chosen such that the IMF component is equally distributed between the four intervals during the statistical time period (dotted line at 25 %). The bar plots give the average distribution during each substorm.

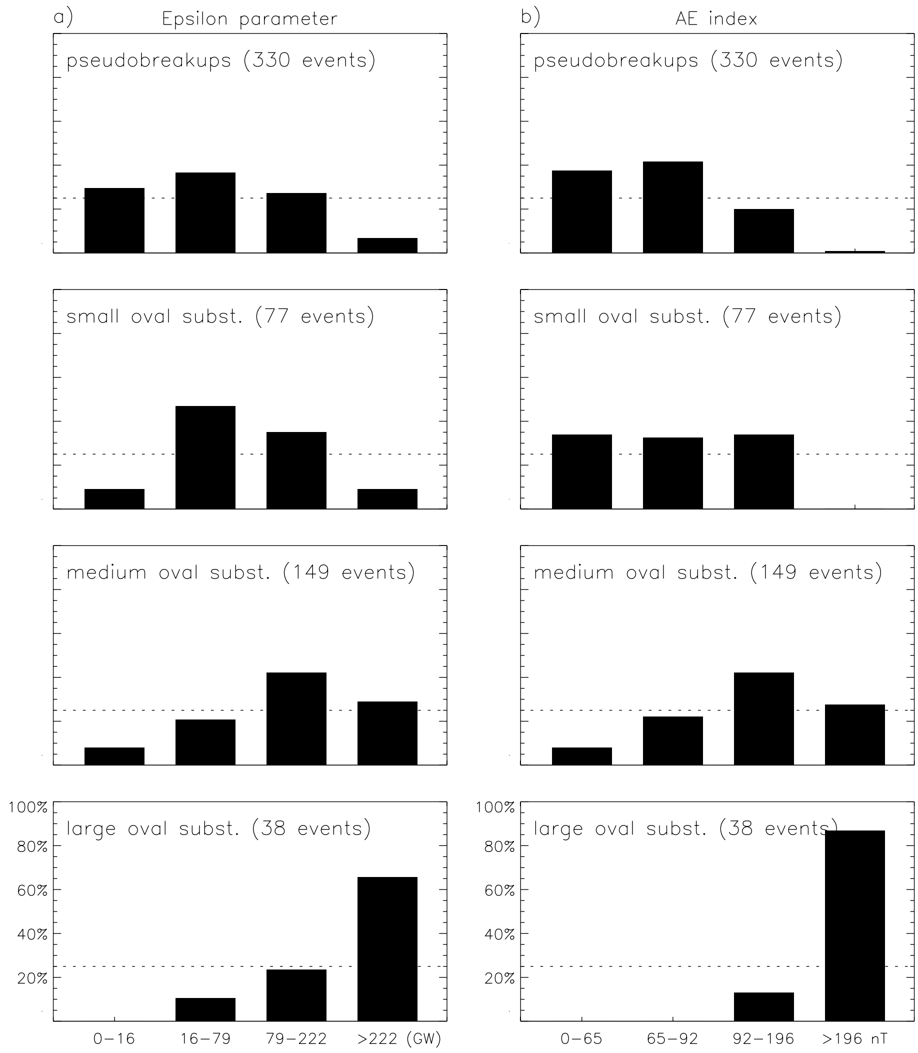
a)
Epsilon parameter
b)
AE index
pseudobreakups (330 events)
small oval subst. (77 events)
medium oval subst. (149 events)
large oval subst. (38 events)
100%
80%
60%
40%
20%
0-16
16-79
79-222
>222 (GW)
0-65
65-92
92-196
>196 nT

Figure 5. The distribution of a) the epsilon parameter and b) the AE index. The figure is done in the same way as Figure 4.

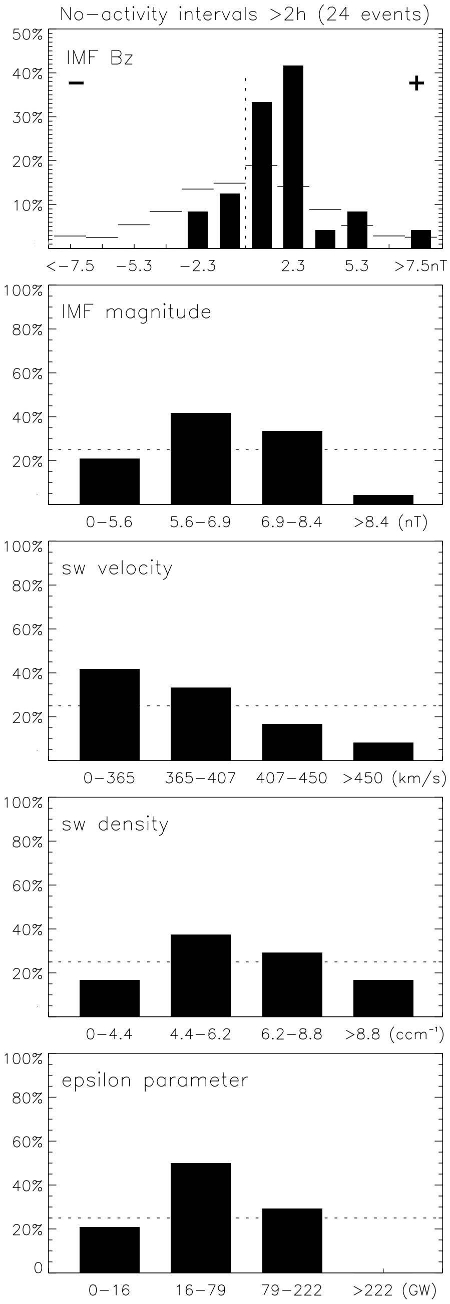
No−activity intervals >2h (24 events)
IMF Bz
−
+
50%
40%
30%
20%
10%
<−7.5
−5.3
−2.3
2.3
5.3
>7.5nT
IMF magnitude
100%
80%
60%
40%
20%
0−5.6
5.6−6.9
6.9−8.4
>8.4 (nT)
sw velocity
0−365
365−407
407−450
>450 (km/s)
sw density
0−4.4
4.4−6.2
6.2−8.8
>8.8 (ccm⁻¹)
epsilon parameter
0
0−16
16−79
79−222
>222 (GW)

Figure 6. The distribution of solar wind parameters for the time intervals (at least 2 hours long) where no auroral activity (pseudobreakups, substorms, small splits, clear polar arcs and all unclear substorm and polar arc events) is seen on the UVI images. The times where no UVI images are available plus 2 hours before and after are excluded. The plots are produced in the same way as the plots in Figure 1 to 5.

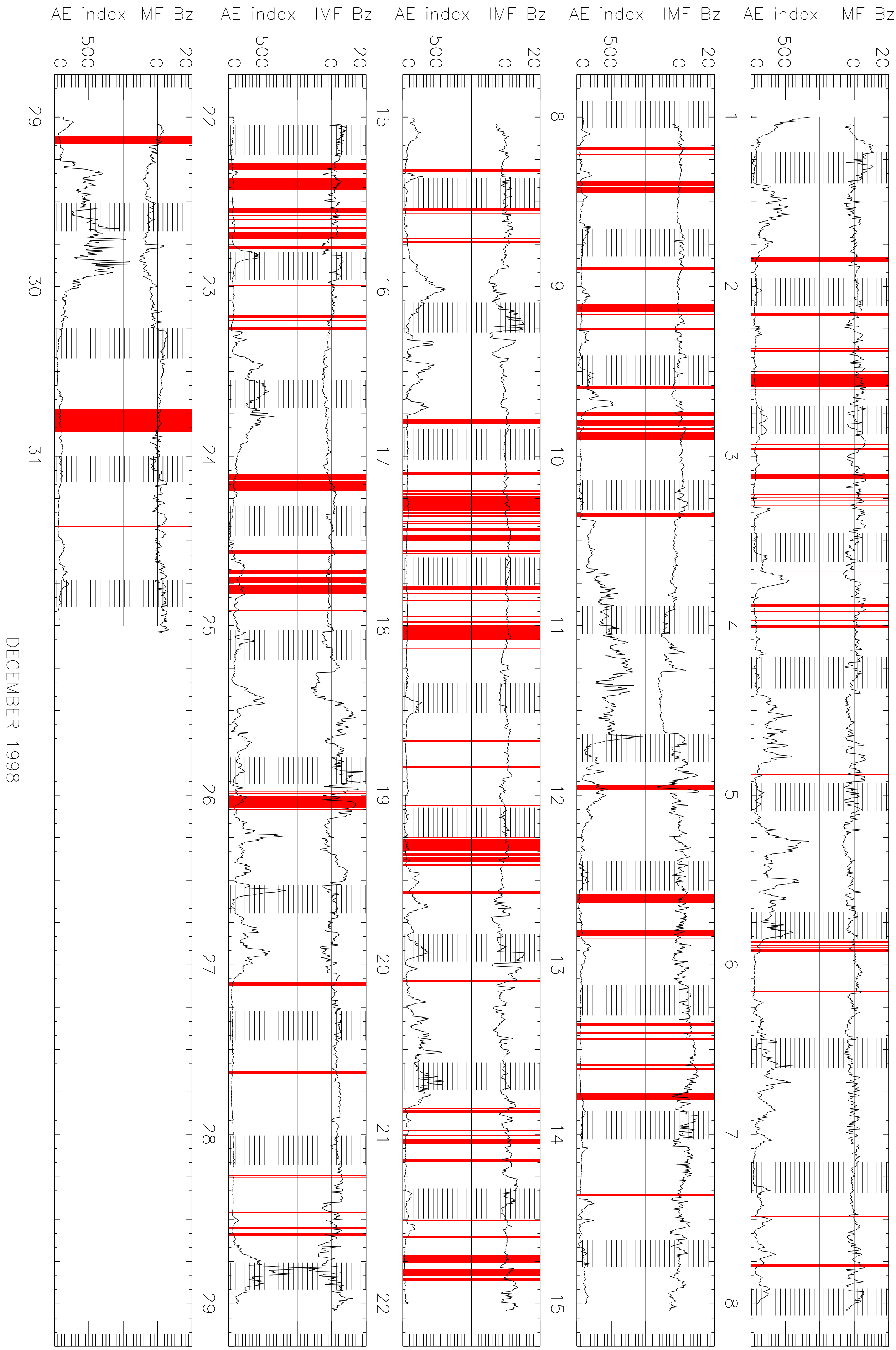
AE index
IMF Bz
DECEMBER 1998

Figure 7. Overview plot over one month with all pseudobreakups found in the Polar UV images (gray bars) overlaid on IMF B_z (nT) (with a propagation time approximated by 1 hour) and AE index values (nT). The fasciated bars mark the times where no UV images are available.

Table 2. Number of substorms (in percentage) with a pseudobreakup occurring up to an hour before or after the substorm

pseudobreakups before	Substorm type	pseudobreakups after
73 % (56 pb's)	small-oval substorm	32 % (25 pb's)
31 % (47 pb's)	medium-oval substorm	25 % (37 pb's)
5 % (2 pb's)	large-oval substorm	24 % (9 pb's)
17 % (20 pb's)	shrinking-oval substorm	31 % (36 pb's)
41 % (15 pb's)	expanding-oval substorm	8 % (3 pb's)

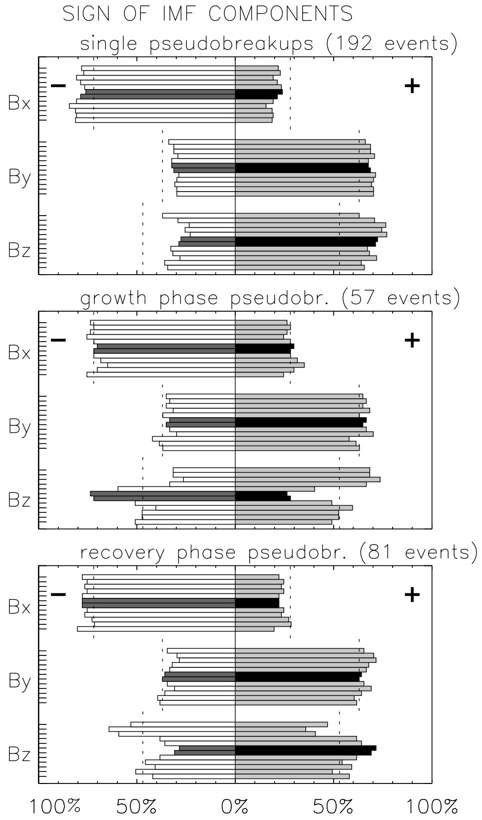
SIGN OF IMF COMPONENTS
single pseudobreakups (192 events)
growth phase pseudobr. (57 events)
recovery phase pseudobr. (81 events)
Bx
By
Bz
−
+
100%
50%
0%
50%
100%

Figure 8. The distribution of IMF B_x,B_y and B_z as percentages of events for different groups of pseudobreakups. The figure is done in the same way as Figure 1.

Table 3. Percentages of pseudobreakups with IMF B_z sign changes occurring within one hour before and after onset

	B_z sign change before onset		B_z sign change after onset	
pseudobreakup type	southturn	northturn	southturn	northturn
single pb's:	20 %	34 %	36 %	19 %
growth phase pb's:	52 %	16 %	19 %	53 %
recovery phase pb's:	24 %	43 %	45 %	25 %

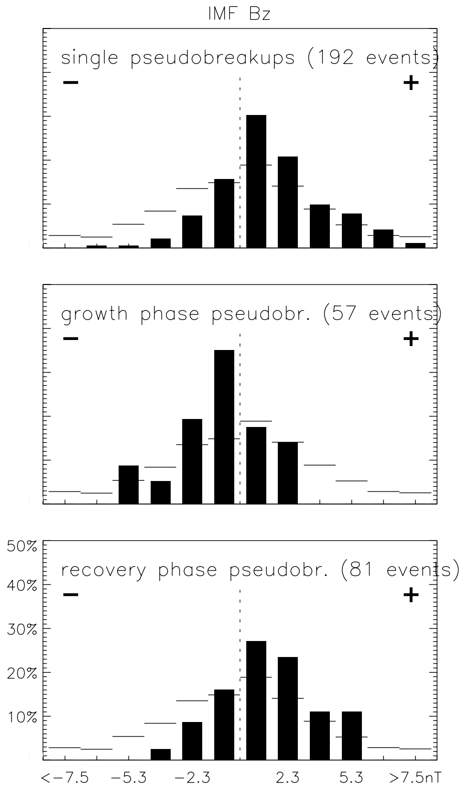

IMF Bz
single pseudobreakups (192 events)
−
+
growth phase pseudobr. (57 events)
−
+
recovery phase pseudobr. (81 events)
−
+
50%
40%
30%
20%
10%
<−7.5
−5.3
−2.3
2.3
5.3
>7.5nT

Figure 9. The distribution of IMF B_z as percentages of events for different groups of pseudo-breakups. The figure is done in the same way as Figure 3.

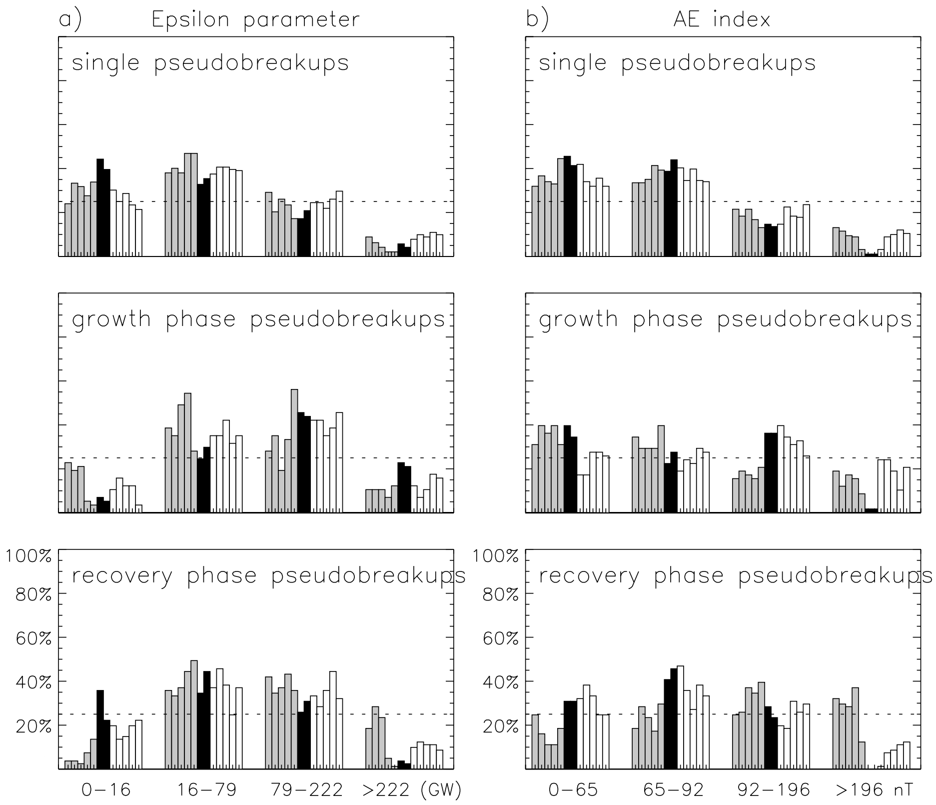
a) Epsilon parameter
b) AE index
single pseudobreakups
growth phase pseudobreakups
recovery phase pseudobreakups
100%
80%
60%
40%
20%
0-16
16-79
79-222
>222 (GW)
0-65
65-92
92-196
>196 nT

Figure 10. The distribution of a) the epsilon parameter and b) the AE index for the different pseudobreakup types. The different magnitude ranges are chosen such that the parameter values are equally distributed between the four intervals during the statistical time period (dotted line at 25%). The distributions are given for the event start (left black bar), the average value during the event (right black bar) the hourly averaged values up to 5 hours before the event (gray bars) and the hourly averaged values up to 5 hours after the events (white bars).

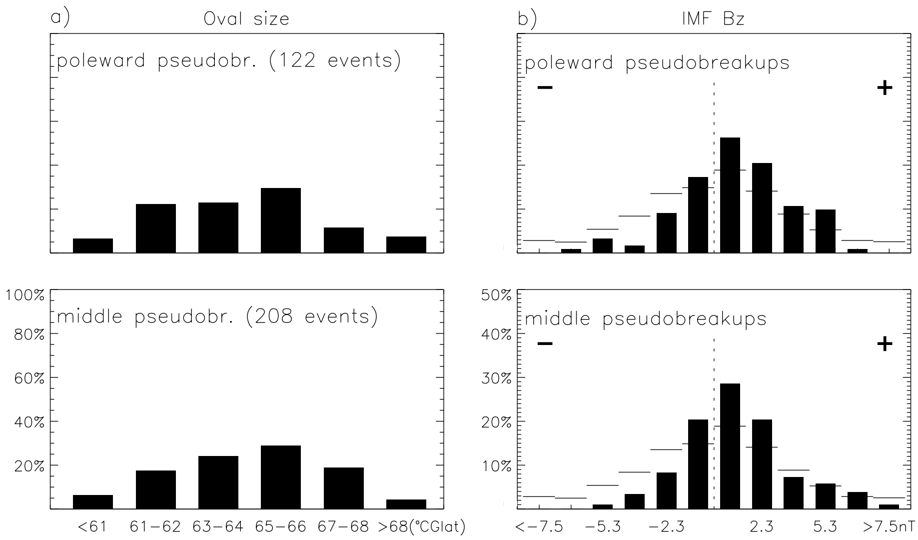

Figure 11. The distribution of a) the equatorward oval boundary location at
b) the IMF B_z component as percentages of events for poleward and middle pseud
Figure 11b is done in the same way as Figure 3.

Table 4. Main characteristics of the different auroral phenomenon

auroral phenomenon	IMF B_z	IMF magnitude	sw velocity	sw density	epsilon/AE index
clear polar arcs:	north	**high**	**high**	average	average
no activity:	zero	*low*	*low*	*low*	*low*
pseudobreakups:	zero	*low*	*low*	*low*	*low*
substorms:	south	average	average	average	**high**

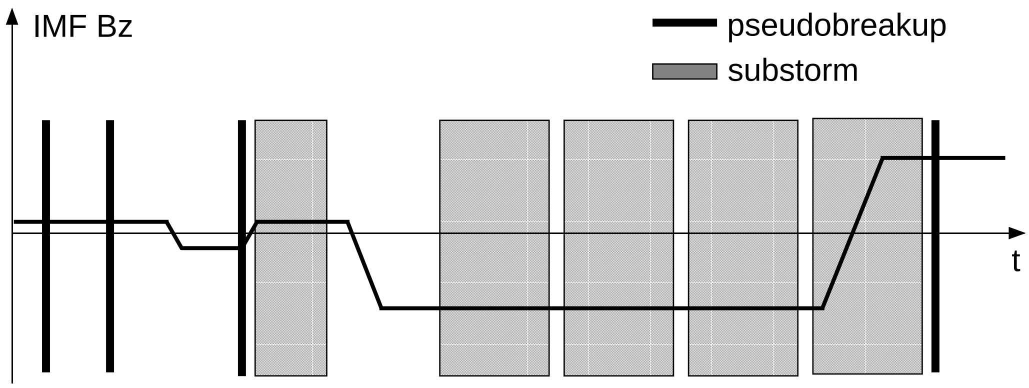

Figure 12. The occurrence of pseudobreakups with respect to IMF B_z and substorms.